"Optoelectronic optimization of Photocatalytic processes for wastewater treatment"

"Thesis submitted in partial fulfillment of the requirement for the PhD Degree issued by the Universitat Politècnica de Catalunya, in its Electronic Engineering Program"

Tecilli Tapia Tlatelpa

Director:

PhD. José Luis Romeral Martínez

Co-Director:

PhD. Jose Francisco Trull Silvestre

Terrassa, Barcelona. September 2019

Abstract

Water pollution is an alarming problem that endangers the health of all living beings. The textile industry is listed as one of the most contaminating industries, since in order to carry out its dyeing and finishing processes, it requires a large amount of water resources; by decades, this industry has used Advanced Oxidation Processes (AOPs), since they have several advantages (e. g. destruction of toxic substances, reduction of heavy metals, allowing their use in conjunction with other processes, among others). Among the AOPs, heterogeneous photocatalysis stands out for its high efficiency for the removal of contaminants, including azo dyes.

In order to perform a photocatalytic process, it is necessary to have a photoreactor, which will require a photocatalyst and at least one light source that activates the catalyst. This type of photoreactors can present several problems, such as the use of high cost photocatalysts, the generation of toxic byproducts in some low photocatalysts, the high electrical consumption caused by the use of traditional lighting sources and even difficulties with the geometry of the photoreactors.

Hence the scientific community has tried to optimize the photocatalytic processes, some scientists have worked in the generation of new photocatalysts to be able to use them in wavelengths generated by low cost lighting sources (e. g. visible light), nevertheless, which in many times it increases the price of the photocatalyst. Another approach is to reduce electricity consumption by opting for the replacement of traditional lamps with low consumption lighting, for example, LED lighting; However, this substitution is currently done arbitrarily, so sometimes some authors doubt the ability to use these sources in this type of process. Moreover, when trying to improve the lighting sources, the photoreactor can be altered, so it is important to take into account its characteristics in order to achieve a significant improvement.

This thesis focuses on an optoelectronic optimization to improve the efficiency of the lighting sources used in photocatalytic reactors. For this, a methodology has been generated to calculate LED arrays using uniform irradiance models, this irradiance must be homogeneous, with enough energy to photoactivate the catalyst with the aim to replace the traditional lamps, avoiding the chemical alteration of the photocatalysts; Likewise, a photocatalytic reactor has been designed and implemented on a laboratory scale with ultraviolet illumination adjusted to its characteristics (i.e. geometry, dimensions, among others) to work with a low cost photocatalyst (TiO_2) in the decolorization of wastewater with textile dyes. Finally, in-situ monitoring has been designed and implemented in order to analyze the decolorization of textile water, this type of monitoring avoids the collection of water samples during the process, without altering the geometry of the reactor or reducing the volume of treated water in the reactor.

Keywords

Ultraviolet Light Emitting Diode	*Heterogeneous Photocatalysis*	*In- situ monitorization*
Uniform Irradiance Models	*Azo dyes*	*Optical monitoring*
Advanced Oxidation Process	*Titanium Dioxide*	*Scattering*

Acknowledgements

To the Universitat Politècnica de Catalunya, especially to my supervisor Dr. Jose Trull for his priceless advices, unending support and effort during these years and Dr. Luis Romeral for his time, constant guidance and advices that helped me bring this study into success.

To the staff of the Laboratory of Environmental Pollution Control from Institute of Textile Research and Industrial Cooperation of Terrassa (INTEXTER), particularly to Dr. Valentina Buscio, for her expertise, guidance to understanding the photocatalytic processes, words of encouragement and teach me to use the laboratory material resources.

To the Mexican Consejo Nacional de Ciencia y Tecnología, for having given me the opportunity to accomplish my Doctoral studies through the scholarship No. 417993. As well as the Secretaría de Educación Pública de México for the scholarships No. BC-5242, No. BC-6585 and No. BC-8128.

TABLE OF CONTENTS

List of Tables

List of Figures

ACRONYMS AND DEFINITIONS

AOPs	Advanced Oxidation Processes
BOD	Biochemical Oxygen Demand
CdS	Cadmium Sulfide
COD	Chemical Oxygen Demand
CEN	European Committee for Standardization
GaP	Gallium Phosphide
LED	Light Emitting Diode
INE	National Institute of Statistics
TiO_2	Titanium Dioxide
TOC	Total Organic Carbon
UNECE	United Nations Economic Commission for Europe
UNGA	United Nations General Assembly
UV	Ultraviolet
ZnO	Zinc Oxide

Chapter 1. INTRODUCTION

1.1 Research topic

Water is essential for living beings, although three quarters of the surface of the Earth are considered covered with water, not all can be used for human consumption.

Since 2010, the United Nations General Assembly (UNGA) recognized the human right to have sufficient, clean and accessible water for its use. The increasing volume of population and industrial development during the last decades has caused a high consumption of water resources that negatively affect the environment, since they generate large amounts of contaminants and waste, which end up contaminating rivers, lakes, and oceans[1].

The wastewater comprises different inorganic and organic contaminants, at the industrial level, some of the waste are an excess of production of dangerous chemical substances[2].

Some solutions to this important environmental problem have been aimed at making an intelligent consumption of resources, as well as developing methodologies that help eliminate water pollution; therefore, the scientific community is continuously working on the creation of separation techniques and methods for the destruction of pollutants.

In order for these techniques to be used, the chemistry of the water to be treated must be taken into consideration, since the processes for their purification are different and depend on the type of contaminant they contain. Water contaminated by human activity generally responds to biological treatment plants, activated carbon methods or traditional disinfection treatments (e.g. chlorination, oxidation, ozonation, among others); however, some of these procedures are not adequate according to regulations for subsequent discharge to the drainage or collectors[2].

Several countries are using wastewater for their irrigation systems (in some countries they represent approximately 7%), but this requires regulation in these waters, which is why the European Union has stipulated the directive 2000/60/CE, where the maximum and minimum values for the content of minerals, ions, and pathogens in water are established to be considered potable[3].

1.1.1 Water Pollution: Textile Industry

The United Nations Economic Commission for Europe (UNECE) has indicated that 20% of wastewater comes from the fashion industry, it is the second CO_2 emitter, and generates more than 21,000 million waste and garbage annually. Since this industry requires 150 - 300L of water to produce one kilogram of textile products[4–6].

The textile industry is a sector that most influences the production of wastewater[7,8].Textile wastewater is commonly intensely dyed and contains high concentrations of organic substances derived from various residues of dyes and different chemical additives[8,9].

This industry uses more than 100,000 different dyes, of which it is estimated that almost 280,000 tons are lost in the textile effluents every year[7,9,10]. Approximately 70 % of these dyes are synthetic azo dyes, and it is estimated that about 800,000 tons are produced annually[9,11]. Azo dyes are widely used because of their high reactivity and color resilience[12,13]. The azo dyes are characterized by nitrogen-nitrogen double bonds the so-called azo bonds (-N=N-)[14].

The biggest danger of textile wastewater is that it ends up spilling into rivers, lakes, mangroves or any other aquifer, causing severe damage to these ecosystems, as has happened with places like Bangladesh[4].

Nowadays a greater amount of clothing is produced at low price, since demand has increased; between 2000 and 2014, the volume of clothing dyed doubled and this phenomenon will continue to occur in coming years[15].

The National Institute of Statistics (INE) in conjunction with the Spanish Intertextile Council of the year 2000, estimates that Catalonia has 65% of the textile activity in Spain, Valencia with 25% and 10% is distributed throughout the rest of the country. The dyeing and finishing sectors have great relevance in Catalonia and the Valencian Community, due to the fact that the greater amount of textile activity is concentrated in these two zones[16].

According to the data provided in 2001 by the Catalan Water Agency, extracted from the Declarations of Water Use and Consumption presented by companies annually, 30% of textile companies discharge 60% of their wastewater when they have been treated; the remaining 70% declared that 36% of wastewater does not have any treatment system, but their waste is discharged to the sanitation system to be treated by the municipal wastewater

treatment plant. Therefore, only 10% of companies dump their waste without any treatment, which would represent 18% of the wastewater generated by the Catalan textile industry[16].

The textile industry has two major problems, its high water consumption, and the complexity to treat wastewater. As this sector performs primary, secondary and advanced treatments to eliminate organic matter, solids that have not been eliminated during the process chain[17].

1.2 Research problem

1.2.1 Techniques for the treatment of textile wastewater

There are different techniques for the treatment of textile wastewater, and they can be classified as shown in **Fig. 1-1** [18]:

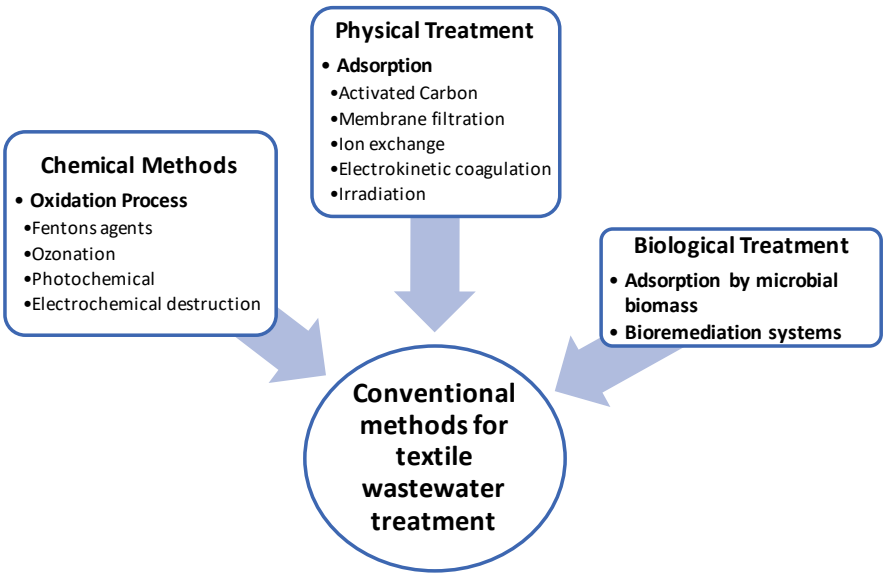

Fig. 1-1. Conventional methods for textile wastewater treatment.

Each of these methods have their advantages and disadvantages. There are some disadvantages that are common in these techniques, for example, the generation of sludge and the high cost of the process, either because of the cost of the chemical agent or because of the electrical cost[18], For this reason during the last years different techniques have been generated for the treatment of textile effluents, focusing mainly on the elimination of dyes, since this process entails greater difficulty.

1.2.2 Advanced Oxidation Processes

There are methods of low cost and high removal of contaminants, which minimize the use of chemicals improving the environmental impact; this type of techniques stand out for their effectiveness and are called Advanced Oxidation Processes (AOPs), they are especially useful before a biological treatment (pretreatment), for the treatment of pollutants resistant to biodegradation or as after-treatment to improve water characteristics[19–22].

The Advanced Oxidation Processes are based on the generation of strongly oxidizing species, the most successful are those that originate hydroxyl radicals (OH•), since they have a high oxidation potential (2.8V)[23].

In order to classify the AOPs can be from the use or not of sources of lighting in the process, resulting in photochemical and non-photochemical processes, in **Fig. 1-2** some of the most commonly used are indicated[24].

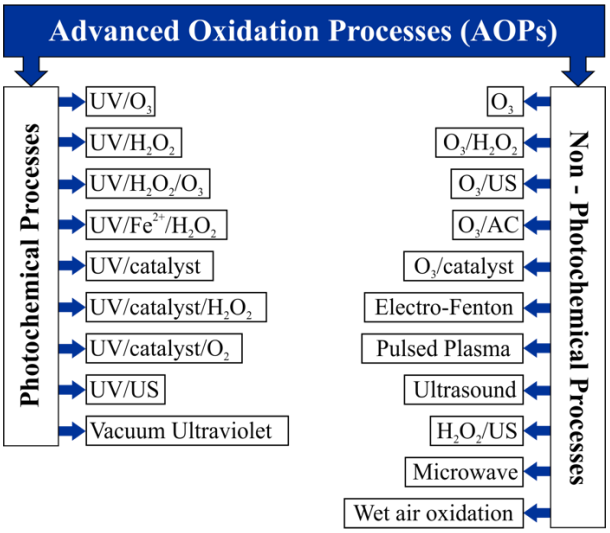

Fig. 1-2. AOPs Classification.

The photochemical processes established for the degradation of pollutants in aqueous media are based on providing enough energy (photons) to the compounds to reach excited states for the time necessary to form reactions. These photons are absorbed by molecules, excite electrons forming free radicals and create other reactions. According to the Planck equation traditional methods that use ultraviolet (UV) radiation have more energetic photons.

For the mineralization and degradation of azo dyes AOPs are commonly used[20–22]. In order to investigate the effectiveness of a photochemical AOP, it is important to consider the following points[25,26].

1. The ability to absorb ultraviolet radiation by the compounds to be degraded.
2. The quantum yield of degradable compounds.
3. Stability and easy photodegradation of degradable products.

The advantages and disadvantages of the AOPs, can be summarized in **Table 1-1** [27]:

Table 1-1. Advantages and disadvantages of AOPs.

Advantages	Disadvantages
• Destruction of toxic substances forming harmless compounds. • Organic substances (simple or complex) are broken down into water, CO_2 and inorganic acids. • Reduction of heavy metals (toxic). • Operate at room temperatures (25 – 80 °C). • They can be used in conjunction with other processes.	• The use high cost reagents. • The process can form intermediate byproducts. • The catalyst can be deactivated during the process.

However, despite these limitations, techniques involving ozonation and UV irradiation are commercialized[19,25,28].

1.2.3 Heterogeneous Photocatalysis

Amongst the AOPs, heterogeneous photocatalytic processes highlight due to their high efficiency in the removal of contaminants, including synthetic dyes[29,30]. In order to carry out photocatalytic processes, a reactor, ultraviolet light sources and photocatalyst are mainly required[31]. Nonetheless, each of these elements may present some drawback.

1.2.3.1 Photocatalyst

Several semiconductors have been used for the degradation of compounds, among them the photocatalyst with the best results is Titanium Dioxide (TiO_2), while Zinc Oxide (ZnO), although it obtains degradations similar to those of TiO_2, with lower cost it is less safe, because, it has a weak chemical stability. Semiconductors such as Cadmium Sulfide (CdS) or Gallium Phosphide (GaP) absorb large fractions of the solar spectrum, but in heterogeneous photocatalysis processes undergo degradation during different catalytic cycles. Finally, other

semiconductors have high cost or are toxic and therefore its use for water treatments is not recommended[25,27,32].

1.2.3.2 UV sources

The conventional mercury lamps (low, or medium pressure) are the most popular lamps for the use of photocatalysis, nevertheless, they waste between 60 – 80 % of their electrical energy in heat and infrared radiation and their lifetime is typically 10,000 - 15,000 hours and they need a large amount of energy for their operation[33].

1.2.3.3 Reactor

The design of photocatalytic reactors is related to two major difficulties, a) ensure the perfect contact between catalyst and water (i.e. the catalyst can be, immobilized or suspended), b) the lighting of the catalyst particles, since it is related to the catalyst bandgap and its position. Some of the intrinsic design parameters are flow distribution, reactor geometry, mass transfer, and catalyst interaction[34].

In conclusion, with the aim to optimize the efficiency and decrease the cost of treated water from heterogeneous photocatalysis processes it is necessary to generate modifications in the main elements involved in photocatalytic processes. In order to realize an optimized reactor, it is necessary to eliminate the traditional sources by sources with low consumption with the aim to decrement the energy consumption, besides, these new sources must provide the necessary energy to photoactivate the photocatalyst; it is also important to consider the type of catalyst used, to prevent the generation of toxic byproducts.

1.3 Hypotheses

In order to solve the presented research problems, the following hypotheses were formulated for this research work:

1. The reduction of the energy consumption of traditional sources can be done by replacing the low consumption sources adapted to the characteristics of the reactor.
2. Using uniform irradiance models it is possible to generate enough ultraviolet radiation required to use with low cost photocatalysts.
3. The decrease of the degradation time can be achieved by taking the lighting to the geometry of the photocatalytic reactor.
4. Using the optical phenomena of photocatalytic processes it is possible to estimate the chemical state of the process.

1.4 Aim and objectives

The aim of this thesis is to **improve energy efficiency, as well as to optimize the ultraviolet illumination of photocatalytic processes. This objective is approached considering the structure of the reactor, the uniform UV-illumination and the photocatalyst.** In addition, an optical setup will be implemented to obtain measurements to estimate the chemical status of the process.

In order to successfully achieve this aim, the following specific objectives are proposed.

- The research, and the characterization of efficient ultraviolet sources to perform photocatalysis.
- Design and modeling of a system for the generation of uniform ultraviolet lighting with high energy efficiency.
- Design and implementation of a photocatalytic photoreactor with optimized lighting.
- The research, design and implement an optical system for the estimation of the textile dyes degradation in photocatalytic processes.

1.5 Outline of the chapters

In order to cover the exposed objectives, this thesis is divided into different sections, ordered as it follows:

Chapter 2 presents a brief review of the state of the art of heterogeneous photocatalytic processes, detailing different problems that nowadays have been tried to solve.

Chapter 3 describes the characterization of traditional sources and LEDs, as well as the methodology that was implemented for the generation of ultraviolet sources with uniform irradiance.

Chapter 4 presents the design and implementation of the photocatalytic reactor with optimized illumination, moreover, the results obtained using the reactor for decolorization of azo dyes are presented.

Chapter 5 shows the degradation results obtained when there are temperature variations in the uniform irradiance system.

Chapter 6 introduces the design and implementation of the online monitoring system in photocatalytic minireactors, to estimate the decolorization of azo dyes in real time.

Although each chapter include a partial conclusion focused on its respective topic, in **Chapter 7** a general conclusions and future work are presented. Additionally, this chapter also offers the contributions resulting from this research work.

Chapter 2. HETEROGENEOUS PHOTOCATALYSIS

The mechanism of photocatalysis begins when a chalcogens semiconductor is irradiated with photons that have energy greater than or equal to that of its band gap (Band Gap). At that moment, a photon absorption occurs and electron / hole pairs (e^-/h^+) are created inside the photocatalyst, which are separated into free electrons in the Conduction Band (e_{CB}^-) and gaps in the Valence Band (h_{VB}^+). This dissociation of charges induces the redox potential, because the holes have oxidant capacity, and the electrons take part in the reduction reactions (see **Fig. 2-1**)[28].

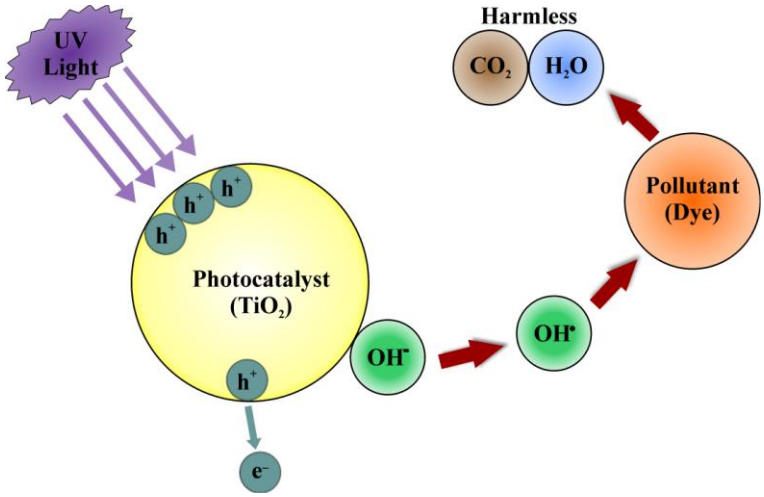

Fig. 2-1. Photocatalytic Process.

According to different studies, heterogeneous photocatalysis can be used to oxidize organic, inorganic compounds, and even treat heavy metals; for that reason, these types of processes are interesting and innovative for the treatment of contaminated water. Nevertheless, after years of research it has been stated that the main drawback to the use of AOPs is the high cost of using reagents as well as excessive energy and electricity consumption to use the lamps or generate ozone[25,32].

2.1 Photocatalysts

A fundamental task to take advantage of heterogeneous photocatalysis is the choice of the catalyst, since it must be activated by light. The catalysts represent an extensive class of semiconductor materials capable of having photocatalytic applications[35].

For a semiconductor to be cataloged as an ideal photocatalyst, it must have the following qualities[27]:

- Photostability
- Chemical and biologically inert nature
- Availability and low cost
- Ability to absorb reagents under efficient photonic activation

Table 2-1 shows the main semiconductors used as photocatalysts, moreover a price comparison of the various catalysts for photocatalysis can be made and ordered according to the wavelength at which they work, to evaluate the possibility of using them either in photocatalysis with conventional lamps, sunlight, among other sources.

Table 2-1. Characteristics of different photocatalysts.

Photocatalyst	Wavelength (nm)	Energy (eV)	Cost (USD/kg)	Zone
SnO_2	318	3.9	60 – 120	Ultraviolet
ZnS	344	3.7	0.6 – 0.9	
$SrTiO_3$	365	3.4	10 – 50	
$BaTiO_3$	375	3.3	15 – 25	
TiO_2	388	3.2	1.5 – 2	
ZnO	390	3.2	0.952 – 1.146	
WO_3	443	2.8	900 – 974	Visible
$FeTiO_3$	443	2.8	1.5 – 2	
CdS	497	2.5	500 – 1000	
Fe_2O_3	565	2.2	50 – 100	
CdO	590	2.1	5.5 – 6	
CdSe	730	1.7	300 – 500	Infrared
GaAs	886	1.4	100 – 400	

As can be seen, the cost of the photocatalyst increases as it approaches the visible region of the electromagnetic spectrum that is used during solar photocatalysis. Although these photocatalysts are commercial, many photocatalysts works have been done to modify their characteristics and thus generate better photocatalysts, unfortunately not all of these works have created a low cost photocatalyst and with characteristics superior to those of TiO_2, and although the activation of the catalyst by sunlight could represent a decrease in the energy cost, it also constitutes an investment in the installation costs of solar photoreactors with coolers to reach the optimum working temperature of the photocatalysis.

In the case of photocatalysts other than titanium dioxide (TiO_2) several comparisons have been made to corroborate their mode of working, some of these studies confirmed that zinc oxide (ZnO) exhibits better efficiency than TiO_2 in the photocatalytic degeneration of dyes in aqueous medium. Kormann conducted a comparative study of the photocatalytic activity of TiO_2, Fe_2O_3, and ZnO, and the results showed that ZnO and TiO_2 possess much more photocatalytic activity than Fe_2O_3 in the degradation of chlorinated hydrocarbons; though, ZnO undergoes corrosion with ultraviolet light induced by autooxidation, and this phenomenon is one of those responsible for the decrease of the photocatalytic activity of ZnO until its inactivation [36].

In addition it has been reported that by doping thin films of TiO_2 with different impurities such as Ce, Nb, Fe, Ag, Au by sputtering or implanting Fe in them, both their structure and their optical and photocatalytic properties can be modified, but many of these elements are toxic and can diffuse from the TiO_2 to the environment during the photocatalytic application[32].

Likewise, cadmium sulfide (CdS) and iron oxides, despite having a suitable spectral response for the capture of solar radiation, are not suitable for the realization of this study, since they are not stable throughout the range of pH and undergo photo-corrosion during the process and the cadmium sulfide in its decomposition generates $Cd^{+}{}_2$, cataloged as environmentally harmful[27].

2.1.1 Titanium Dioxide

Titanium dioxide is the most used catalyst in photocatalysis applications due to its high resistance to corrosion, low cost and safety[23,37].

TiO_2 can be found in three crystalline forms, anatase, rutile and brookite, of these phases only the first two have photocatalytic activity, nevertheless, anatase has better yields. Each crystal lattice has its own electronic bands therefore its respective band gap and wavelength for its excitation, being for anatase 3.2 eV at 384 nm and for rutile 3.0 eV at 410 nm[38].

Due to this variation in the behaviors, a photocatalyst has been created by mixing these anatase and rutile forms in proportion 80/20, 75/25, or 70/30%. The commercial TiO_2 is called Degussa P-25 and their activation zone is ≤ 388nm[39].

TiO_2 has some disadvantages, such as the difficult recovery of the suspension due to its small size (specific surface area of 49 m^2/g and a particle diameter of 21 mm) and its insufficient photocatalytic activity with solar radiation. For this reason, during recent years, a lot of research has been carried out to improve the characteristics of this catalyst, which have resulted in various methods of synthesis and doping, in addition to immobilizers and supports to recover the photocatalyst[40,41]

Likewise TiO_2 presents several advantages (i.e. photostability, effective oxidative power, and low or non- toxicity, low cost)[22,37]. Moreover its use in photocatalytic processes has some benefits such as, no addition of chemical products, no generation of wastes (sludges), and its full recovery that can be reused[42,43]. The photocatalytic process can be expressed according to **Eq. 2-1 - Eq. 2-8** [11]:

$$TiO_2 + hv(UV) \rightarrow TiO_2(e_{CB}^- + h_{VB}^+) \quad \textbf{Eq. 2-1}$$

$$TiO_2(h_{VB}^+) + H_2O \rightarrow TiO_2 + H^+ + OH^\bullet \quad \textbf{Eq. 2-2}$$

$$TiO_2(h_{VB}^+) + OH^- \rightarrow TiO_2 + OH^\bullet \quad \textbf{Eq. 2-3}$$

$$TiO_2(e_{CB}^-) + O_2 \rightarrow TiO_2 + O_2^{-\bullet} \quad \textbf{Eq. 2-4}$$

$$O_2^{-\bullet} + H^+ \rightarrow HO_2^\bullet \quad \textbf{Eq. 2-5}$$

$$Dye + OH^\bullet \rightarrow degradation\ products \quad \textbf{Eq. 2-6}$$

$$Dye + h_{VB}^+ \rightarrow oxidation\ products \quad \textbf{Eq. 2-7}$$

$$Dye + e_{CB}^- \rightarrow reduction\ products \quad \textbf{Eq. 2-8}$$

2.2 Ultraviolet Sources

The term photocatalysis is defined by the IUPAC as "the acceleration of a chemical reaction in the presence of a photocatalyst, by excitation of ultraviolet radiation". UV radiation acts as the initiator of the reaction, not as a catalyst, because this radiation is depleted in the process[29–31,44].

As mentioned above, the bandgap of photocatalysts requires ultraviolet light irradiation, which is why there is a vast amount of artificial sources that help generate ultraviolet light. The most used ultraviolet light sources can be grouped into conventional, sunlight, laser and LED[10].

2.2.1 Conventional ultraviolet lamps

In order to describe the behavior of ultraviolet lamps, a division is made with respect to the emission wavelength, where there are black lamps, which emit a long wavelength of UV radiation, and germicidal lamps that emit a long wavelength. Shortwave UV radiation, these can be low or medium pressure lamps[45].

2.2.1.1 Fluorescent lamps

Fluorescent lamps are commonly used in the lighting industry. This type of lamps consists of a glass or quartz tube with two electrodes at each end, with an inert gas (argon, neon, xenon or krypton) containing mercury vapor at low pressure as an active ingredient; a typical mixture contains about 1% or even 0.1% metal vapor, and 99% - 99.9% inert gas.

Mercury emits at UV at wavelengths of 253.7 nm (approximately 65% of the emitted light) and 185 nm (approximately 10% - 20%)[33,46].

The overall efficiency of the conversion of electrical energy into a fluorescent lamp (under optimal conditions) is approximately 28%. Due to the losses in the form of heat in the discharge, the walls and the electrodes, only about 63% of the consumed electrical energy is converted into UV radiation. This type of lamps work best at room temperature and its optimum working range is between 10 and 35 ºC, where the standardized luminous flux reaches approximately 90%. It's useful life depends on the construction and varies from 5,000 to 24,000 h[47].

2.2.1.2 Xenon lamps

Xenon and mercury-xenon lamps operate at very high pressure and temperature, therefore, they have to be handled with care to avoid thermal stress and contamination of the bulb. They produce bright white light that mimics natural light, which is appropriate for applications involving solar simulation (projection systems, absorbance, fluorescence). Mercury-xenon arc lamps have mainly the mercury spectrum with a xenon contribution[33].

2.2.1.3 Mercury lamps

They are low pressure lamps, are used in applications that require high spectral purity. These lamps have a long warm-up time before starting to emit. When used with filters they can also provide strong monochromatic radiation at wavelengths of 404.7 and 435.8 nm (violet), 546.1 nm (green), and 577.0 and 579.1 nm (yellow).

2.2.2 Solar light

Currently, there is a low efficiency design of solar capture technology, which leads to capture 0.04% of the original solar photons, added to this, considering that it is only possible to work with 5% of the spectrum of ultraviolet solar radiation reaching the low atmosphere, it is deduced that solar radiation is not very efficient to be used in photocatalysis systems[32].

2.2.3 Ultraviolet LED

UV Light Emitting Diode (LED) has an external quantum efficiency and a life time greater than 100,000 h, which is approximately 100 times longer than an conventional UV lamp; it has a low cost, robustness, compact size, light weight, low consumption, operate at room temperature and produces directional UV light that can be of the desired wavelength. Currently, this ultraviolet source are being widely used in studies of heterogeneous photocatalysis becoming an alternative to conventional ultraviolet lamps[48].

Some of the advantages of LEDs is that they do not require cooling systems to work, in addition you can resort to various assemblies in reactors. On the other hand, being unidirectional, the design of a reactor can achieve a high photocatalytic efficiency avoiding losses of UV light[32,49].

The photocatalysis with UV/TiO_2 uses conventional UV-lamps, which are typically based on low or medium pressure lamps, however due to its disadvantages (i.e. low photonic efficiency, overheating, short lifetime, high energy consumption, toxicity (mercury), low mechanical stability, cooling requirements), in recent years they have been replaced by LED lighting sources[10,50,51].

2.2.4 Comparison of ultraviolet light sources

Table 2-2 shows the comparison of ultraviolet sources that can be used in wastewater treatment.

Table 2-2. Comparison of ultraviolet sources.

Characteristics	LED LED385-33	LP PL-L 18W/10/4P	Xenon UXL-S75XE
Wavelength (nm)	380 – 390	320 – 450	350 – 800
Cost (USD)	8	14	500
Power (W)	0.2	18	80
Current (A)	0.02	0.375	5.4
Voltage (V)	10	58	15
Radiation power in UV (W)		3.5	8
Temperature (ºC)	-30 – 80	20 – 200	20 – 200
Lifetime (h)	100,000	5,000	2,000

While LEDs do not seem to be efficient enough as other sources, studies have shown that for certain applications, the replacement of mercury lamps with ultraviolet LEDs can significantly reduce CO_2 production to 15 tons[10].

For this reason, the European Committee for Standardization (CEN) has prescribed conditions in which photocatalytic surfaces should be irradiated during the photocatalytic efficiency test, and LEDs have been included in the list of irradiation lamps, thanks to their unique properties[45].

In addition, photocatalytic reactors that use traditional UV light sources can waste up to 80% of the light they produce, while the LEDs to emit at specific wavelengths can completely use the light they generate and certain studies indicate that increasing the number and power of the LEDs can get better photocatalytic degradation of pollutants in less time (because these devices do not heat up)[10].

2.3 Photocatalytic Reactors

One of the most outstanding properties is the diameter of the reactor, since it must ensure an adequate relationship between the light source, the concentration of the photocatalyst and the efficiency of the process. The manner in which the radiation affects the reactor and the length of the optical path are essential to determine the optimum concentration of the catalyst and to avoid shielding effector. Another important parameter is the type of material used because they must have a high resistance to degradation and the ability to transmit UV, shortening the list of possibilities. The most common materials are plastics, acrylics and glass (with low content of iron and quartz, the latter being very expensive)[34].

The first investigations in the field of photoreactors were carried out with UV lamps because in this way the experimental conditions can be controlled, besides establishing the wavelength in a specific work zone. Recently, basic research was carried out at the laboratory level for the development of new reactor designs, since commercial prototypes are mainly based on immersion reactors (annular)[32,52].

2.3.1 Classification of photocatalytic reactors

There are several options to classify photoreactors

Catalyst: The photocatalyst may be in suspension or immobilized [51].

- Photoreactors with agitation: They are used for photocatalysts in suspension.
- Photoreactors with supports: They are used for immobilized photocatalysts.

Illumination: UV irradiation is important for the design of reactors[38].

- Ultraviolet lamps: Mercury, low, medium or high pressure xenon lamps are the most popular.
- Solar light: They have different configurations, which will be defined later.
- LEDs: They have different advantages given their small sizes and the ease of coupling provided by this light source.

Source position: Location of the light source with respect to the reactor [29].

- Immersion: The light source is located inside, either centered or surrounding the reaction chamber. Within this type is the immobilizer configuration where the surface of the lamp can also provide additional area for the immobilization of the catalyst (see **Fig. 2-2a**).
- Distributive: The light is distributed to the catalyst, a disadvantage is that the light hits the surface of the catalyst, without limiting the absorption by reagents. There are subtypes that include reflectors and fiber optics (see **Fig. 2-2b**).
- External: The light source is located outside the reaction chamber, decreasing efficiency if the light source and the reactor are not of a single unit (see **Fig. 2-2c**).

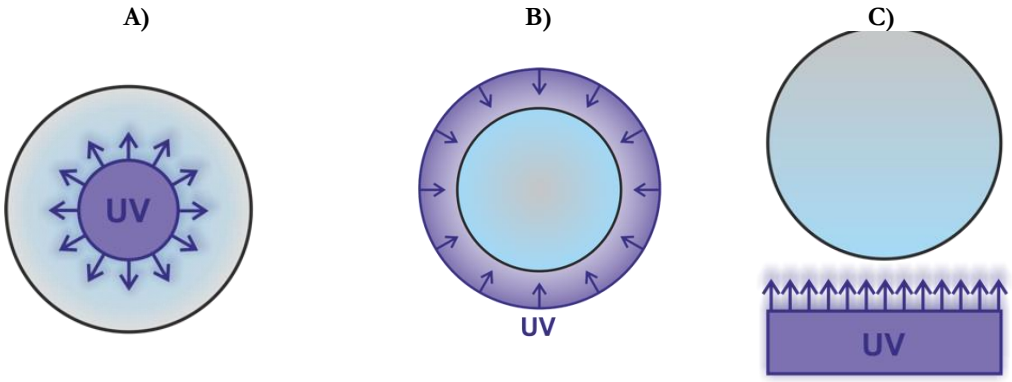

Fig. 2-2. Position of the source in photoreactors. **A)** Immersive, **B)** Distributive, **C)** External.

2.3.1.1 Annular reactor

These reactors the lamp is placed on the central axis of the cylinders (immersive). It has the advantage that practically the total of photons emitted by the lamp reach the medium to be degraded. With the aim to prevent the photons from reaching the external wall of the reactor by a small size in the design, a mirror covering the system can be placed. Sometimes these types of reactors are used for the continuous flow water process, in this case, it is recommended that contaminated water passes more than once through the length of the reactor to ensure that all the effluent is treated[52].

2.3.1.2 Reactor with catalyst in suspension

The most popular ones use the suspended catalyst in a flow that resides in an annular space surrounded by an ultraviolet source, nonetheless the latest studies have created thin films that contain the catalyst and thus it is easier to recover after the water process. This type of reactors considers the mass balance important since it involves the conversion and the agitation of the tank [47,49].

2.3.1.3 Multilamp reactor

This type of equipment is widely used when the source of radiation are low pressure or fluorescent lamps, since they have low power. The configuration consists of several lamps in parallel to generate high radiant fluxes. Multilamp reactors have several geometries, most are cylindrical and the lamps are tubular, sometimes the reaction chamber is coated with reflective surfaces to take better advantage of the radiant flow. This type of reactors are used industrially in the field of water purification [52].

2.3.1.4 Reactor with filtering membranes

The design of these reactors is almost similar to the annular reactors, however they use a microporous membrane at the outlet of the water flow, this membrane has the adequate dimensions to retain the catalyst inside the reactor, which makes them more efficient to recover the catalyst. Tubular designs of this type have been applied in river water treatments[11].

2.3.1.5 Reactor with immobilized catalyst

These designs are cylindrical and the catalyst is immobile on a support to prevent its separation. A modification has large supports (the size of the reactor wall) and supports can be fiber mesh, or glass beads. These reactors use only one lamp and in the case of large reactors a matrix of lamps is used to generate sufficient radiation[47].

2.4 Operation parameters of photocatalytic processes

2.4.1 Catalyst concentration

The concentration of the catalyst intervenes directly with the photocatalytic reaction rate, in a higher concentration is more probably a turbulence phenomenon, since efficient absorption of photons is prevented, therefore it is important to verify the amount of photocatalyst when used in suspension.

At high concentrations the catalyst produces a slow reaction rate, and it is advisable to use a concentration close to the steady state point, so that the catalyst can be fully illuminated[28].

In addition, the intrinsic characteristics of the catalyst influence the photocatalysis process. The size of the particles improvement the generation of pairs e^-/h^+; However, if the particles have defects, they can sometimes reduce the efficiency of the process. While the properties in its texture contribute to improve the relationship between the catalyst and the species to be degraded[53].

2.4.2 Contaminant Concentration

Generally, the kinetics of photocatalytic processes follow a Langmuir-Hinshelwood mechanism (see **Eq. 2-9**)[54]:

$$r = K\theta = \frac{k(KC)}{1+KC} \qquad \textbf{Eq. 2-9}$$

where k is the true velocity constant; K is the equilibrium adsorption constant and C is the instantaneous concentration. The values of k and K have a direct relationship with the rest of the operating parameters of the photocatalytic processes, as well as by the contaminant.

2.4.3 pH

The pH affects the contaminant and the catalyst, a change in pH may imply improvements in the efficiency of the removal of organic contaminants (in the presence of TiO_2) without affecting the reaction rate [25].

2.4.4 Temperature

Because of photonic activation, photocatalytic systems do not require heating and work at room temperature. At low temperatures (-40 to 0 ºC) and at very high temperatures (> 80 ºC) the photon activity decreases, therefore, the optimum temperature to work is an average temperature (20 to 80 ºC)[23].

2.4.5 Radiant Flow

The reaction rate is proportional to the radiant flow, given the photoinduced characteristic of the photocatalytic process, where the pairs (e^-/h^+) are consumed mainly by the chemical reagents instead of by the recombination rate. An approximate value of 25 mW/cm^2 has been calculated in laboratory experiments using TiO_2[28].

It should be considered that very intense radiant flows can increase the temperature of the photocatalyst, therefore it is important to avoid the use of too energetic lamps, especially when working with small photoreactors[22].

2.4.6 Quantum yield

It is defined as the ratio of the reaction rate in the molecules per second (or in moles per second) to the efficient photon flux in photons per second (or in Einstein per second). Its theoretical maximum value is equal to 1. It is directly related to the instantaneous efficiency of a photocatalytic system. The knowledge of this parameter is fundamental to compare the activity of different photocatalysts in the same reaction, estimate the relative viability of different reactions and calculate the energy efficiency of the process as well as its cost[23].

2.4.7 Oxygen concentration

The oxygenation is necessary for a total mineralization and its concentration disturbs the speed of reaction, since oxygen allows the reception of electrons that give rise to the development of photocatalytic reactions by decreasing the recombination of the pairs (e^-/h^+), nonetheless, some authors ensure that high concentrations of oxygen slow down the rate of degradation[27].

2.5 Conclusions

In this chapter the main elements that make up the photocatalytic processes were presented, as well as their operation parameters.

The elements that make up these processes are closely related. The lighting (**Table 2-2**) depends on the type of photocatalyst (**Table 2-1**) and the geometry of the reactor (**Fig. 2-2**); the photocatalyst (suspension or immobilized) affects the geometry of the reactor and therefore the reactor must have the characteristics according to the type of photocatalyst and the light source.

Chapter 3. MODELING SOURCES AND DESIGN OF ULTRAVIOLET ILLUMINATION

3.1 Introduction

In the last years some authors[10,32,51,55–57] proposed the use of UV-LEDs to carry out the photocatalysis, most of the current studies focusing on the direct replacement of the conventional ultraviolet lamp by LED arrays[49,58,59] without any discussion regarding which is its most optimal distribution, in fact the number of LEDs changes considerably in the different proposals. Hence, finding a way to determine the minimum number of LEDs and its geometrical distribution needed to replace effectively the conventional UV lamp source is a question of potential interest.

In this chapter we approach this problem by considering several important factors, which should be taken into account, such as the location and angle of position of the light source, the distance between this and the reactor and, mainly, the generation of a uniform irradiance pattern similar to that provided by the lamp to be replaced. Inasmuch as photocatalysis operation depends crucially on the photonic efficiency (the measure of the rate of reaction divided by the incident light intensity), it is necessary to design the geometry of LED arrays to obtain the desired value of irradiance as well as uniform field illumination[32,55].

With the aim to achieve this goal we use reported mathematical models for LEDs[60–62] to calculate the irradiance of a specific type of arrays and find an implemented geometry to obtain uniform illumination at a selected plane[63,64].

3.2 Irradiance models

The replacement of conventional lamps by LEDs is performed imposing the condition that the irradiance generated by both sources at the central region of a given reactor should be equal. Any significant difference between the irradiance of the new source with regard to the current to be replaced, will lead to a performance loss of the photocatalytic process. Due to the distinct emission properties of each source in terms of radiated intensity and angular emission pattern a direct comparison of the emission of a single LED with an UV lamp is not adequate. Therefore, it is necessary to determine the optimum array configuration (i.e., geometry and number of LEDs), which must be used to obtain equivalent irradiances.

3.2.1 Irradiance model for single LED

LED arrays will be considered formed by individual emitters with identical properties (i.e., wavelength, radiant flux, irradiance). Due to their optical characteristics, LEDs of spherical encapsulation and without encapsulation cannot be considered Lambertian emitters, so their irradiance distributions are not directly proportional to the cosine of the angle of view. Nevertheless, it is possible to obtain a practical approximation of the irradiance distribution $E(r,\theta)$ for a LED[60], given by:

$$E(r,\theta) = E_0(r)\,cos^m(\theta) \qquad \textbf{Eq. 3-1}$$

where $E_0(r)$ is the irradiance (W/cm^2), r is the distance (cm) on axis and θ the view angle (deg).

The reported values of m by different authors vary, Chen [60] report that $m > 1$, while Moreno [64] report that $m > 30$, which indicates large variations in the emission properties of each LED. However, at the specific view angle where the irradiance takes a value equal half to its maximum value, $\theta = \theta_{1/2}$, $\mathrm{E(r,\theta) = E_0(r)/2}$, m for **Eq. 3-1** can be expressed by:

$$m = \frac{-\ln 2}{\ln(\cos\theta_{1/2})} \qquad \textbf{Eq. 3-2}$$

Considering a single LED placed at the position (x_0, y_0) in the $z_0 = 0$ plane, the irradiance at a given point with coordinates (x, y) placed in a plane at distance z (see **Fig. 3-1** for a schematic representation) is obtained by writing **Eq. 3-1** in Cartesian coordinates (x,y,z):

$$E(x,y,z) = \frac{z^m I_{LED}}{[(x-x_0)^2 + (y-y_0)^2 + z^2]^{(m+2)/2}} \qquad \textbf{Eq. 3-3}$$

where, $E(x,y,z)$ is the irradiance distribution, I_{LED} is the intensity (mW/sr) of the LED, z is the distance (cm) between the LED and the target (reactor), and m is given by **Eq. 3-2**.

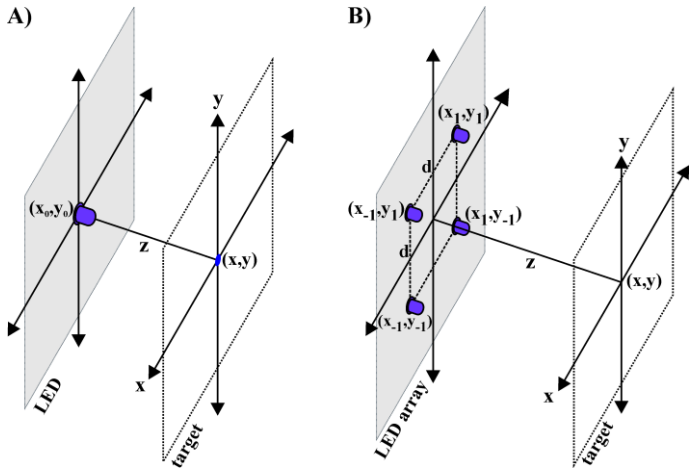

Fig. 3-1. Schematic representation of the LED configuration and illumination plane. **A)** Location of a single LED, **B)** Square LED array 2x2.

Since the irradiance model is based on the superposition of the emissions of each individual LEDs, the equation modeling distinct LED arrays will vary according to the particular distribution of the LEDs in the plane $(x_0, y_0, 0)$.

3.2.2 Irradiance model for Two LEDs Array

The irradiance of a pair of LEDs (see **Fig. 3-2**) is produced by the sum of the irradiances of each LED and can be calculate by:

$$E(x,y,z) = z^m I_{LED}\{[(X_a)^2 + y^2 + z^2]^{-(m+2)/2} + [(X_b)^2 + y^2 + z^2]^{-(m+2)/2}\} \quad \textbf{Eq. 3-4}$$

where,

$$X_a = x - (d/2) \quad \textbf{Eq. 3-5}$$

$$X_b = x + (d/2) \quad \textbf{Eq. 3-6}$$

The optimum distance between elements can be calculated by:

$$d = z(4/m + 3)^{1/2} \quad \textbf{Eq. 3-7}$$

where z is the distance between the center of the array to the target.

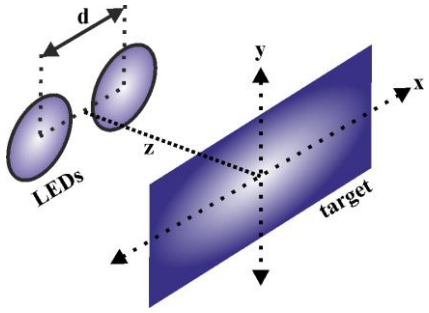

Fig. 3-2. Irradiance pattern of two LEDs.

3.2.3 Irradiance model for Linear LED Array

The irradiance of a linear array (see **Fig. 3-3**) is given by the sum of each of the LEDs to make up the array:

$$E(x,y,z) = z^m I_{LED} \left\{ \sum_{n_0=1}^{N} \left[(X^2 + y^2 + z^2)^{-(m+2)/2} \right] \right\} \quad \textbf{Eq. 3-8}$$

where,

$$X = x - (N + 1 - 2n_0)(d/2) \quad \textbf{Eq. 3-9}$$

and N is the number of LEDs.

The optimal distance between elements depends on the number of elements in the array, if the array has 3 LEDs, the distance can be calculate by:

$$d = z(12/m + 3)^{1/2} \quad \textbf{Eq. 3-10}$$

For arrays with more than 4 elements the distance will be calculate by:

$$d = z(3.2773/m + 4.2539)^{1/2} \quad \textbf{Eq. 3-11}$$

The requirements imposed by **Eq. 3-11** guarantee that more than 98% of the generated irradiance of the array is found at the central region of the target reactor.

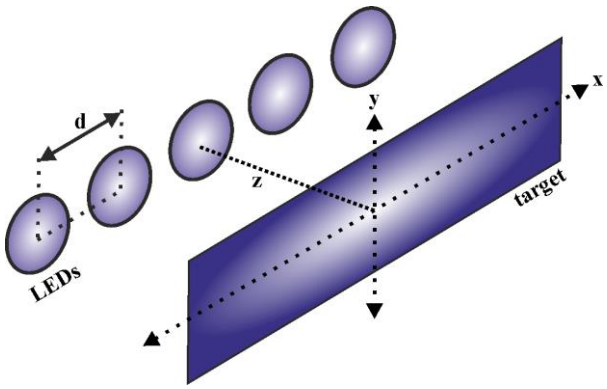

Fig. 3-3. Irradiance pattern of linear LED array.

3.2.4 Irradiance model for square LED array

The most used array for lighting panels and for large lamps is the square geometry, whose irradiance $E(x,y,z)$ is the sum of the matrix consisting of MxN LEDs. As proposed by Moreno[64] the separation between LEDs in this configuration can be properly selected with the aim to obtain a uniform irradiance $E(x,y,z)$ for a given distance z (see **Fig. 3-4**):

$$E(x,y,z) = \mathrm{z}^m I_{LED} \times \left\{ \sum_{n=1}^{N} \sum_{m_0=1}^{M} \frac{1}{[X^2 + Y^2 + z^2]^{(m+2)/2}} \right\} \qquad \textbf{Eq. 3-12}$$

where,

$$X = x - (N + 1 - 2n)\left(\frac{d}{2}\right) \qquad \textbf{Eq. 3-13}$$

$$Y = y - (M + 1 - 2m_0)\left(\frac{d}{2}\right) \qquad \textbf{Eq. 3-14}$$

and N, M are the number of LEDs for the x-axis and y-axis respectively.

For arrays of dimensions 2x2 (see **Fig. 3-1B**), the distance d between each LED is equal for the *x* and *y* axis, and is given by:

$$d = z\left(\frac{4}{m+2}\right)^{1/2} \qquad \textbf{Eq. 3-15}$$

and for arrays with superior dimensions, distance *d* is given by:

$$d = z\left(\frac{1.2125}{m-3.349}\right)^{1/2} \qquad \textbf{Eq. 3-16}$$

The requirements imposed by **Eq. 3-16**, guarantee that more than 97% of the generated irradiance of the array is found at the central region of the target reactor.

In order to obtain a particular irradiance value at a given point (x,y,z) (i.e., taken the plane z at the reactor position) using **Eq. 3-2** to **Eq. 3-16** imposing as initial condition the desired value of irradiance $E(x,y,z)$ at that point; the number and position of the LEDs (N, M, x_0 and y_0) in the plane $z = 0$ will then be changed until obtaining the final configuration that satisfies the imposed conditions.

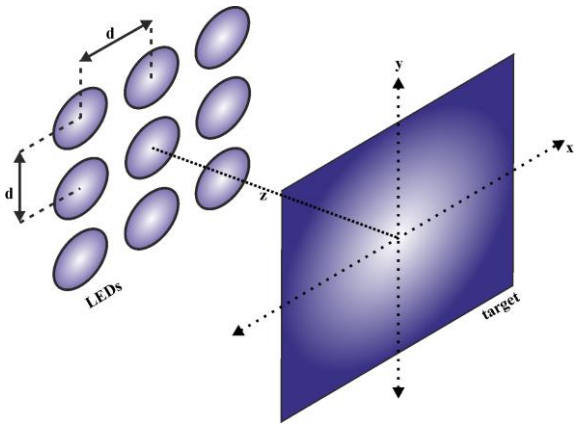

Fig. 3-4. Irradiance pattern of square LED array.

3.2.5 Hexagonal LED Array

The hexagonal array (see **Fig. 3-5**) is formed similarly to the square array, nevertheless, the number of LEDs is calculated by:

$$LEDs = (N \times M) - 0.25[2M + (-1)^M - 1] \quad \textbf{Eq. 3-17}$$

where *N*, *M* are the number of LEDs for the *x*-axis and *y*-axis respectively.

The irradiance of a hexagonal array is given by the sum of the irradiances of each its elements:

$$E(x,y,z) = z^m I_{LED} \left\{ \sum_{m_0=1}^{M} \sum_{n_0=1}^{N_-} \left[(X^2 + Y^2 + z^2)^{-(m+2)/2} \right] \right\} \quad \textbf{Eq. 3-18}$$

where,

$$X = x - (N_+ - 2n_0)(d_x/2) \quad \textbf{Eq. 3-19}$$

$$Y = y - (M + 1 - 2m_0)\left(d_y/2\right) \quad \textbf{Eq. 3-20}$$

and the $N \pm$ term is:

$$N_\pm = N[(-1)^{m_0} \pm 1]/2 \quad \textbf{Eq. 3-21}$$

For arrays of dimensions 2x1 or 1x2, the distances among elements are:

$$d_x = z(4/m + 2)^{1/2} \quad \textbf{Eq. 3-22}$$

$$d_y = \frac{z(12)^{1/2}}{2(m+2)^{1/2}} \quad \textbf{Eq. 3-23}$$

For arrays with more elements the optimal distances are:

$$d_x = z(1.2125/m - 3.349)^{1/2} \quad \textbf{Eq. 3-24}$$

$$d_y = \frac{z(3.6375)^{1/2}}{2(m-3.349)^{1/2}}$$ **Eq. 3-25**

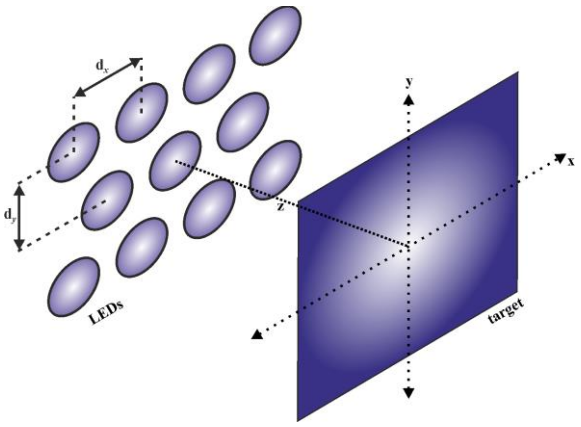

Fig. 3-5. Irradiance pattern of hexagonal LED array.

3.2.6 Irradiance model for Radial LED Array

Other of the most popular arrays is the radial LED array (see **Fig. 3-6**). The total irradiance of this array is given by the sum of the irradiances of its elements, with $N \geq 3$ LEDs.

$$E(x,y,z) = z^m I_{LED}\left[\sum_{n_0=1}^{N}(X^2+Y^2+z^2)^{-(m+2)/2}\right]$$ **Eq. 3-26**

where,

$$X = x - \rho\ \cos(2\pi n_0/N)$$ **Eq. 3-27**

$$Y = y - \rho\ \sin(2\pi n_0/N)$$ **Eq. 3-28**

ρ is the radius of the array, this radius change to produce the uniform irradiance in the center of the pattern, and is given by **Eq. 3-29** for arrays with N = 3 LEDs or **Eq. 3-30** when the array has N > 3 elements,

$$\rho = z(2/m+2)^{1/2}$$ **Eq. 3-29**

$$\rho = z(1.851/m+2.259)^{1/2}$$ **Eq. 3-30**

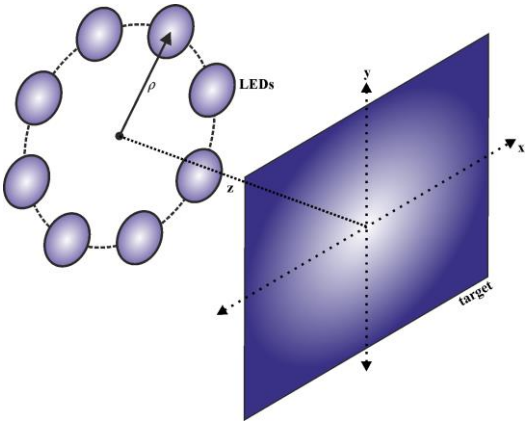

Fig. 3-6. Irradiance pattern of radial LED array.

3.2.7 Irradiance model for Radial with Central LED Array

The radial with central LED array is a modification of the previous array (see **Fig. 3-7**), nonetheless, the equation to calculate de uniform irradiance change, because the central LED alters the homogeneity of the pattern. This array depends of the number of its LEDs $(N+1 \geq 4)$.

$$E(x,y,z) = z^m I_{LED} \left\{ \sum_{n_0=1}^{N} \left[(X^2 + Y^2 + z^2)^{-(m+2)/2} \right] + \phi (x^2 + y^2 + z^2)^{-(m+2)/2} \right\} \quad \textbf{Eq. 3-31}$$

where,

$$X = x - \rho \cos(2\pi n_0 / N) \quad \textbf{Eq. 3-32}$$

$$Y = y - \rho \sin(2\pi n_0 / N) \quad \textbf{Eq. 3-33}$$

ρ is the radius of the array,

$$\rho = z(4/m + 2)^{1/2} \quad \textbf{Eq. 3-34}$$

ϕ is the relative flux $(\phi = \Phi_{central}/\Phi_{ring})$ of the central LED $(\Phi_{central})$ respect to the power (Φ_{ring}) of one LED over the ring. The optimal relative flow depends on the number of LEDs and is given by:

$$\phi = N(m + 2/m + 6)^{(m+6)/2} \quad \textbf{Eq. 3-35}$$

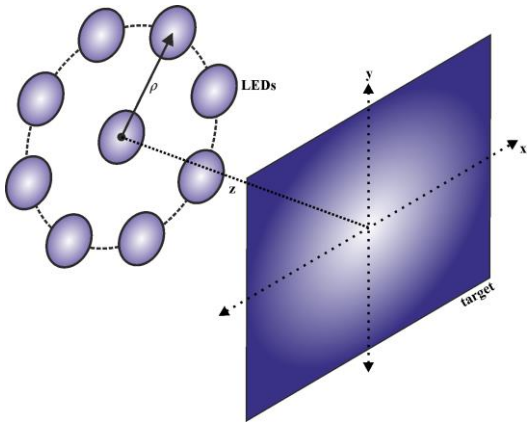

Fig. 3-7. Irradiance pattern of radial with central LED array.

In this chapter will be explained the methodology to calculate different UV-LED array to replace the conventional UV-lamps in a cylindrical photocatalytic reactor of diameter 6.5 cm and height 8 cm.

3.3 Methodology

3.3.1 Characterization of UV sources

In order to replace conventional lamps with optimized LED arrays, the current reactor sources (low pressure mercury UV-lamps) and four different commercial LEDs were characterized. To characterize the optical power of the sources, a thermopile S120VC was used. Spatial characterization of the sources was performed by measuring the optical power as a function of the angle and of the distance to the source at a constant room temperature of 22 ºC.

Table 3-1. Data of sources provided by the manufacturers.

Characteristics	UV- lamp	UV - LEDs			
Model	Philips PLL 18W/10/4P	XSL-370-5E	XSL-375-5E	VL380-5-15	LED385-33
Peak wavelength (nm)	360	370	375	380	385
Radiated Power (W)	3.5	0.006	0.006	0.007	0.011
Power dissipation (W)	18W	0.2	0.2	0.2	0.2
Current (mA)	370	50	50	50	50

3.3.2 Proposed algorithm

In order to calculate the smallest number of LEDs for different types of arrays, an algorithm was implemented, this algorithm satisfies the needs of uniform irradiance of the photocatalytic reactor using the uniform irradiance models.

In this research work a cylindrical reactor illuminated from the exterior by sources placed at fixed distance from its center was used. The initial conditions were established by fixing the desired irradiance value (E_{des}) at the plane z corresponding to the distance between the source and the center of the reactor (other options could be adopted for different reactor geometries). Additional input parameters were the data of the individual LEDs (view angle, intensity, and dimensions). E_{des} corresponds to the irradiance value delivered by the UV-lamp measured at the center of the reactor.

With the aim to calculate the dimensions of a square array with uniform irradiance, the algorithm starts by comparing the irradiance of a single LED with E_{des}. In the case of single LED irradiance larger than E_{des} the algorithm stops. Usually this condition will be not met in the first iteration and additional LEDs should be added to form the array. Since this reactor has a defined height and it is desired to obtain a uniform illumination along the vertical direction, the next iteration in the square array algorithm is to place a second LED in this direction, separated from the first LED by a distance d provided by **Eq. 3-15**. The position of the LEDs in the vertical direction is optimized to maximize irradiance and again is compared with E_{des}. If the obtained value is lower than the desired irradiance, a new LED is added also in the vertical direction. The maximum number of LEDs in the vertical position is limited to

the height of the reactor. If the irradiance with the maximum number of LEDs in a single column is still lower than the target value E_{des}, the following iteration consists in the addition of an identical column separated from the first one by the distance given by **Eq. 3-16** (or **Eq. 3-15** if the array is 2x2), and again the position of the array is implemented in order to maximize the irradiance at the target point. The iterations continue adding new columns until the calculated irradiance is larger or equal to E_{des}. Once the algorithm obtains the desired irradiance, it provides the total number of LEDs, specifying the number of elements that should be in *M* and *N*, as well as their optimal distances.

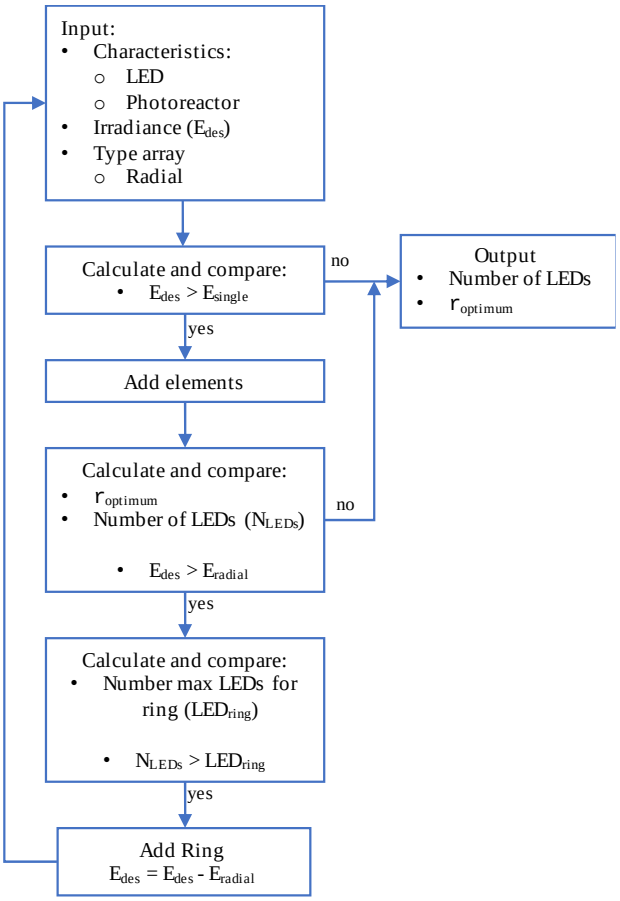

Fig. 3-8. Flowchart of proposed algorithm with radial array.

A similar algorithm can be implemented for other array geometries. For instance, for the radial array distribution the optimum radius can be found and different number of LEDs are added on a given ring by taking in regard its optimum angular position with the aim to maximize its irradiance at the selected point. More rings can be added until the target value is obtained (see **Fig. 3-8**).

3.4 Evaluation Results

3.4.1 Characterization of UV sources

The **Fig. 3-9** shows the relative intensity of the commercial LEDs with the aim to corroborate the data provided by the manufacturer (see **Table 3-1**), both the intensity and peak wavelength differ from producer's data. To make the arrays for the experiments we selected the model LED385-33, because, it has the highest intensity of the UV LEDs.

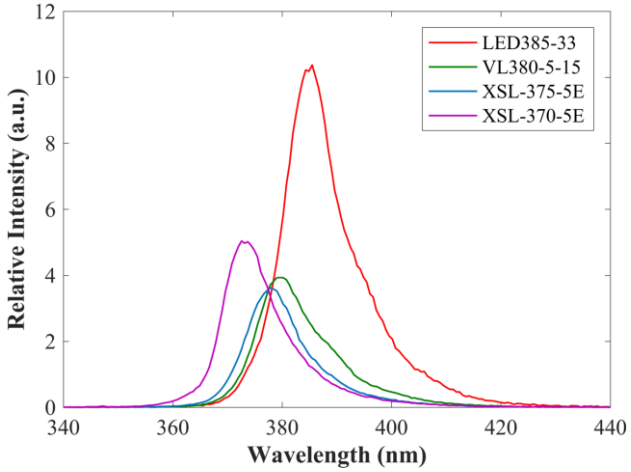

Fig. 3-9. Relative intensity of different commercial UV-LEDs

Angular emission measurements show that the LEDs have a reduced emission angle with respect to the lamps. In addition, these measurements provide the value of the angle (θ) to be used in the determination of the parameter m as given in the **Eq. 3-2**.

The polar plot corresponding to the UV lamp represented in **Fig. 3-10A** shows an angular emission over 360º with an emission pattern which is not homogeneous due to the particular geometry of the lamp, the emission being reduced by 50% when observed in the direction where the two tubes that compose the lamp are aligned. This type of lighting will not use the total irradiance generated by the lamp for the photocatalytic process, since part of the emitted light falls out of the limits of the reactor.

In the case of the single LED, the angular emission also depends on its construction geometry; as can be seen in **Fig. 3-10B**, the light emission is limited to a certain angular range, which is lower than the emission angle of the lamps. Taking **Eq. 3-1** as reference, the maximum emission occurs when the LED emits normally to the surface and decreases as the

angle θ increases. The value of m used in the equations of distribution of irradiance (**Eq. 3-3** and **Eq. 3-4**), is obtained from the half-maximum view angle measured experimentally $\theta_{1/2} = \pm 12º$. For this experiment the result obtained was m = 31.37.

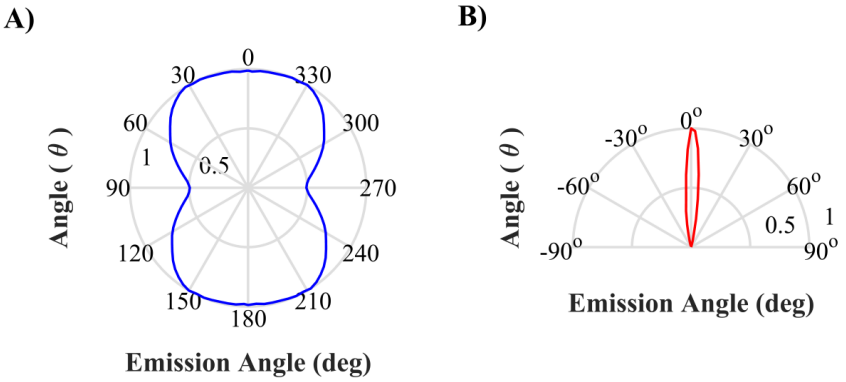

Fig. 3-10. Normalized angular emission of sources measured at a distance of 10 cm from the photodetector. **A)** a low-pressure ultraviolet lamp **B)** An ultraviolet LED, measured at a distance of 10 cm respect to the photodetector.

In order to verify the feasibility of the replacement of conventional UV lamp sources by the use of LED arrays by means of the proposed methodology, two steps were involved. First, the irradiance of an ultraviolet lamp was measured experimentally (along the direction of the maximum emission shown in **Fig. 3-10A**) as a function of the distance from the lamp. These results are plotted in **Fig. 3-11** (circular marks), for distances ranging between 6 – 36 cm. Secondly, the algorithm proposed in the previous section was used to generate the LED arrays matching the measured irradiance of the UV lamp at a specific distance; an square geometry scheme was selected, and once that the features of the arrays were obtained (i.e., their dimensions and number of LEDs) the irradiance values were calculated (**Fig. 3-11,** square marks) in order to compare them with the values of the lamp.

The differences between the irradiances of each light source (**Fig. 3-11**, error bars) are due to that the methodology to generate the arrays has as objective to match or exceed the E_{des} value (i.e., the measured irradiance of the lamp), therefore, for some points an array could provide a higher irradiance than the required. Moreover, with the aim to corroborate mathematically that the results of each source have a direct relation, a trend curve was fitted to each source and the Pearson correlation coefficient was calculated, obtaining a result of 0.99, which verifies that both sources performed similarly and satisfy the Inverse-squared law.

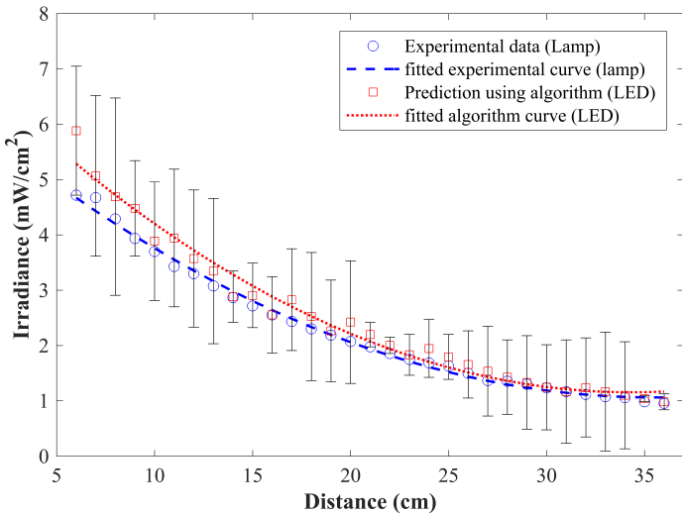

Fig. 3-11. Irradiance of a lamp measured experimentally vs irradiance prediction of different LED arrays using the proposed methodology, at different positions. Fitted curves show the trend of experimental and predicted irradiance. The error bars indicate the difference in irradiance.

The performance of the heterogeneous photocatalysis process is associated to the use of a source of illumination that activates the photocatalyst. For the case of Degussa P-25 titanium dioxide, an ultraviolet source is necessary. **Fig. 3-12** shows the emission spectrum measured experimentally of the two different ultraviolet sources used in this work and their relation to the working area of TiO_2 (defined by the shaded area).

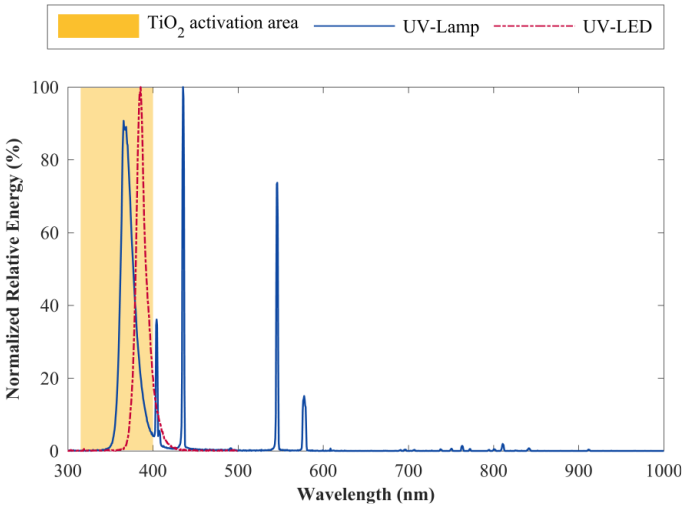

Fig. 3-12. Emission spectra of ultraviolet sources, and its relation to the activation area of TiO_2.

It can be observed that conventional UV-lamps emit over a broader frequency spectrum than the UV-LED, but only a part of the emitted energy falls within the active region of the photocatalyst, representing a waste of energy. As a counterpart, the UV-LED concentrates most of its energy in the working area of the photocatalyst, being highly efficient for the photocatalytic processes. However, since the emitted intensity of a single LED is smaller than the intensity of the UV-lamp, several LEDs are needed to reach the irradiance values of a conventional lamp, being the array configuration a key parameter in order to achieve comparable results.

3.4.2 LED array configuration

The irradiance distribution of the UV-lamps at a distance of 10 cm from the source (corresponding to a transverse plane that crosses the center of the reactor) is shown in **Fig. 3-13A**, depicting a relatively homogeneous illumination with a maximum irradiance of 6 mW/cm^2 at the center, and decreasing to 5 mW/cm^2 towards the edges of the reactor.

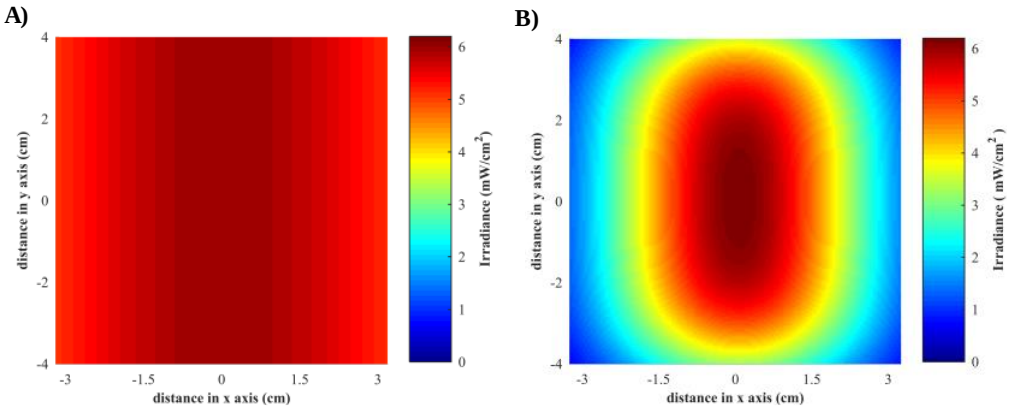

Fig. 3-13. Irradiance distribution of two sources. **A)** UV-lamp at a distance of 10 cm from the source **B)** square array of 5x2 LEDs with d = 1.68 cm between elements, at a distance of z = 8 cm from the source

The selected distance to place the LED arrays was z = 8 cm to the center of the reactor (and not 10 cm as in the case of the UV-lamps by practical purposes in this setup). E_{des} (6 mW/cm^2) was defined by the maximum irradiance value of the UV-lamp at the point (0,0) plotted in **Fig. 3-13A**. The results show that a square array of 2x5 LEDs separated by d = 1.68 cm between elements is needed to obtain the desired irradiance value at the selected point.

In **Fig. 3-13B**, the distribution of irradiance in the transverse plane crossing the center of the reactor is plotted, and the results were obtained using the *m* parameter value obtained from the experimental measurements (*m* = 31.37) and achieving a value of 6.16 mW/cm^2 for the (0,0) point.

Since the emission patterns of the UV-LEDs and the UV-lamp are highly dissimilar (**Fig. 3-10**), it is evident that the irradiance pattern of the sources is not identical (**Fig. 3-13**). However, it can be seen that the main goal of the methodology was achieved, by having generated the same irradiance value for the LED array as for a lamp at the center of the reactor, and most of its physical area is covered by the irradiance pattern.

When the separation between LEDs is less than the optimal (i.e., by reducing their distance), the irradiance is increased but at expense of reducing its irradiation area, leading that the photocatalyst existing inside the reactor is not homogeneously illuminated and hindering its activation. Otherwise, the effect of a larger separation between individual elements results in non-uniform distribution and an overall decrease of the irradiance as well as in the photoactivity of the process.

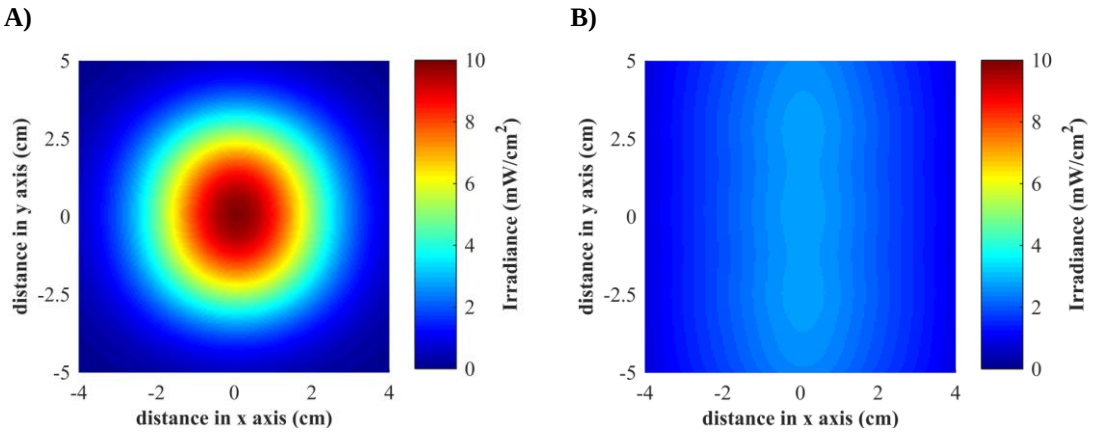

Fig. 3-14. Field of square array of 5x2 LEDs, at distance z = 8 cm from the source, with different distances between LEDs. **A)** space between elements less than optimal, *d* = 1 cm, **B)** space between elements superior to the optimum, *d* = 2.68 cm.

3.4.3 Photoreactor with non-uniform irradiance

The photoreactor to be optimized uses a magnetic stirrer to mix the photocatalyst with the dyed water, in **Fig. 3-15** can be seen that the rotation of the magneto produces a vortex in the reactor center, this vortex is a typical in all reactors with this type of agitation.

A) **B)**

Fig. 3-15. Vortex generated by magnetic stirring. **A)** front view, **B)** Top view.

To perform the optimization of lighting in these reactors, it must be taken into account that the vortex generates absence of water in the center of the reactor, for which reason, it is not advisable to calculate the maximum irradiance at this point, coupled with this, the decrease in volume of the reactor after each sample takes varies the dimensions of the vortex.

Three arrays were generated, providing the greatest amount of irradiance in the lower area of the reactor in order to optimize the lighting of the reactor. To generate the arrays, the maximum irradiance point was calculated evading the empty area of the vortex, and the volume decrease within the reactor was also considered.

3.4.4 LED array implementation

Fig. 3-16 shows the distribution of the implemented arrays. The square LED array of **Fig. 3-16A** replaces a single ultraviolet lamp, only containing 10 LEDs, with a distribution of 2x5 pieces and a distance of 1.68 cm between them. The radial LED array of **Fig. 3-16B** with radius of 2.1 cm, and a separation of 12º between elements, is able to replace the three lamps with a single array of 30 pieces, and has been designed to radiate from the top of the photoreactor. The non-uniform array of **Fig. 3-16C**, replaces a single ultraviolet lamp in vortex reactors, has 12 LEDs, in the upper part of the array it has 6 LEDs with a square distribution and d = 1.25 cm, while in the lower area 6 LEDs have a square distribution with d = 0.8 cm.

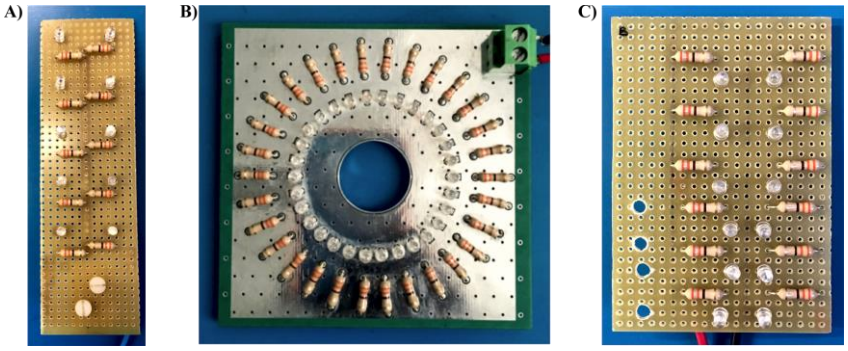

Fig. 3-16. Distribution of the implemented arrays. **A)** Square LED array 2x5, **B)** Radial LED array, **C)** Non-homogeneous array.

3.4.5 Implemented methodology

The algorithm that forms the methodology described in this chapter was implemented and a graphic interface was created in MATLAB® (see **Fig. 3-17**), with the aim to facilitate the insertion and obtaining of the characteristics of the elements of the Array.

In **Fig. 3-17** the titles that are written in blue belong to the input data and the titles in red are the values calculated for the calculated array.

Theta value is used to calculate the *m* value, the radius of the LED is also requested to calculate the minimum possible distance between elements in the different array configurations and in the radial arrangements to avoid overlapping the elements.

The initial coordinates are specified if an array is not required to be centered with respect to the reactor dimensions, the z value is the distance between the LED to the maximum point of the desired irradiance, the Irradiance (E) is the desired irradiance value (E_{des}) and the Reactor dimensions are to calculate the limit dimensions that arrays can have.

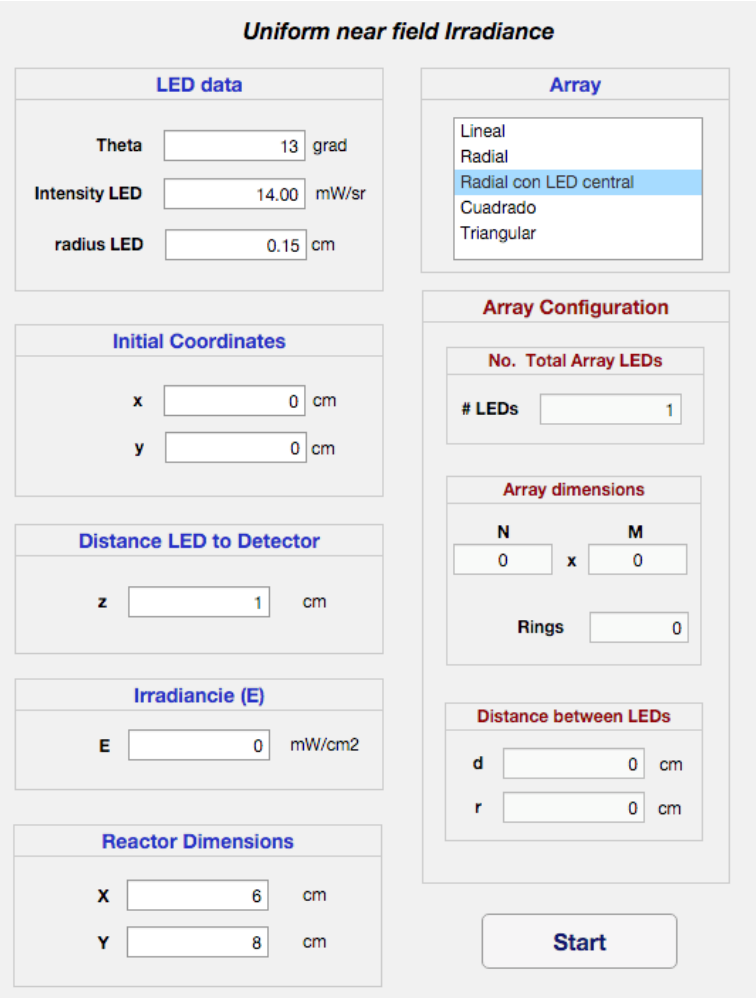

Fig. 3-17. Graphical interface for application of the algorithm to calculate the characteristics for LED arrays with uniform irradiance.

3.5 Discussion and conclusions

This chapter explains the generation of the methodology that gives a solution to the problem of uniform illumination of the photocatalytic reactors, because currently the replacement of conventional lamps is carried out without taking into account the geometry of the reactor.

The characterization of UV sources has shown that although the lamps have emission angles greater than LEDs, the emitted energy is not always used by the photoreactor, either they emit in wavelengths where there is no photocatalyst activity or by the geometry of the reactor;

and the LEDs because their structure can be adapted to specific distances or areas of the reactor, and all their emission energy can be used by the photocatalyst.

Furthermore, it was shown that it is possible to create a methodology using uniform irradiance models to calculate the minimum number of LEDs and generate the irradiance equivalent to a conventional lamp.

Besides, another way to optimize photoreactors on a laboratory scale is the total utilization of the emitted ultraviolet light. When the lamps are not perfectly aligned with the structure of the reactor, the ultraviolet light not incident in the reactor can be reused using panels that reflect UV, however, these panels have an extremely high cost so it is more profitable to place arrays optimized on all photoreactor faces.

Chapter 4. PHOTOCATALYTIC REACTORS AND PHOTOCATALYTIC TESTS

4.1 Introduction

Textile industry is one of the largest consumers of water, mainly due to their finishing processes, such as dyeing, printing and subsequent washing steps. In general terms between 150 and 350 L of water are required to produce a kilogram of textile product[4]. In addition, wastewater from textile industry contains different types of dyes and chemical additives, which cannot be easily degraded by conventional processes[5,6]. Currently, the treatments applied in order to process textile effluents are based on biological or physical-chemical processes. In general, the conventional biological treatment provides good chemical oxygen demand (COD) removal, but low efficiencies in color removal, due to the chemical stability and resistance to microbiological attack of dyes. Otherwise, the coagulation-flocculation treatment can remove color completely, but generates a sludge which requires an additional treatment to be destroyed [9,65].

Conventional lamps are being replaced by sources with low energy consumption and within this context the rapid development of LEDs over the last years have opened up new opportunities[10,45]. Nevertheless, it is still under discussion the possibility of using UV-LEDs as efficient sources of ultraviolet light with enough energy and with the proper frequency range to be used during oxidation processes. Additionally, we could take advantage of its directionality to obtain maximum illumination towards the catalyst, of its reduced cost, compact size, lightweight, lower operating temperature and long lifetime.

4.2 Methodology

4.2.1 Reagents

The materials used for this experiments were: i) Orange PX-2R dye (Reactive Orange 13), with CAS number 12225-85-3, molecular weight 762.03 g/mol; ii) titanium dioxide powder (TiO_2) from the Sigma-Aldrich manufacturer (CAS number 13463-67-7), with particles of 21 nm, surface area of 35 – 65 m^2/g and a molecular weight 78.87 g/mol.

4.2.2 Light sources

Two types of light sources were used: i) a low pressure mercury UV-lamp, Philips PLL 18W/10/4P UVA, with peak wavelength at 360 nm, radiated power of 3.5 W and power dissipation of 18 W, operated at 370 mA. ii) UV-LEDs, Roithner LaserTechnik LED385-33 UVA, with peak wavelength at 385 nm, radiated power of 11 mW and power dissipation of 200 mW, operated at 50 mA.

4.2.3 Photocatalytic reactors

For the measurements of the decolorization efficiency and energy consumption from the different sources, a photocatalytic reactor was built using a 250 mL borosilicate vessel and a magnetic stirrer to mix the TiO_2 photocatalyst. Four different configurations were tested, one using UV-lamps and three with different UV-LED array configurations (the distribution of LEDs was obtained using the algorithm explained in the chapter 3).

Fig. 4-1A shows the schematic photoreactor with three UV-lamps arranged at 120º around the vessel, at a distance of 10 cm from the center of the reactor. The schematic photoreactor of **Fig. 4-1B** has three square UV-LED arrays (**Fig. 3-16A**), placed 120º around the container, at a distance of 8 cm from the center of the reactor. **Fig. 4-1C** shows the schematic photoreactor using the UV-LED radial array (**Fig. 3-16B**), placed in the upper part of the photoreactor, at a distance of 10 cm with respect to the bottom of the vessel, and finally **Fig. 4-1D** is the schematic square&radial photoreactor, combining the radial and square arrays(**Fig. 3-16A-B**).

The geometric configuration and the separation between UV-LEDs was selected with the aim to obtain an illumination as uniform as possible in the reactor with intensities comparable to that given by the UV-lamps used in the first configuration (**Fig. 4-1A**).

4.2.4 Photocatalytic degradation experiments

In order to simulate the effluents after the dyeing process, 250 mL of distilled water were mixed with 0.1 g/L of Orange PX-2R dye. Before photodegradation, the solution was mixed with 1 g/L of photocatalyst in suspension and then the mixture was put on magnetic stirrer in complete darkness for 30 minutes to ensure the adsorption of the dye on the surface of the catalyst. After 30 minutes, the UV-light source was turned on with the mixture in

constant agitation. The treatment was performed for 8 hours, and samples of were taken from the reactor every hour in order to determine the efficiency of the process.

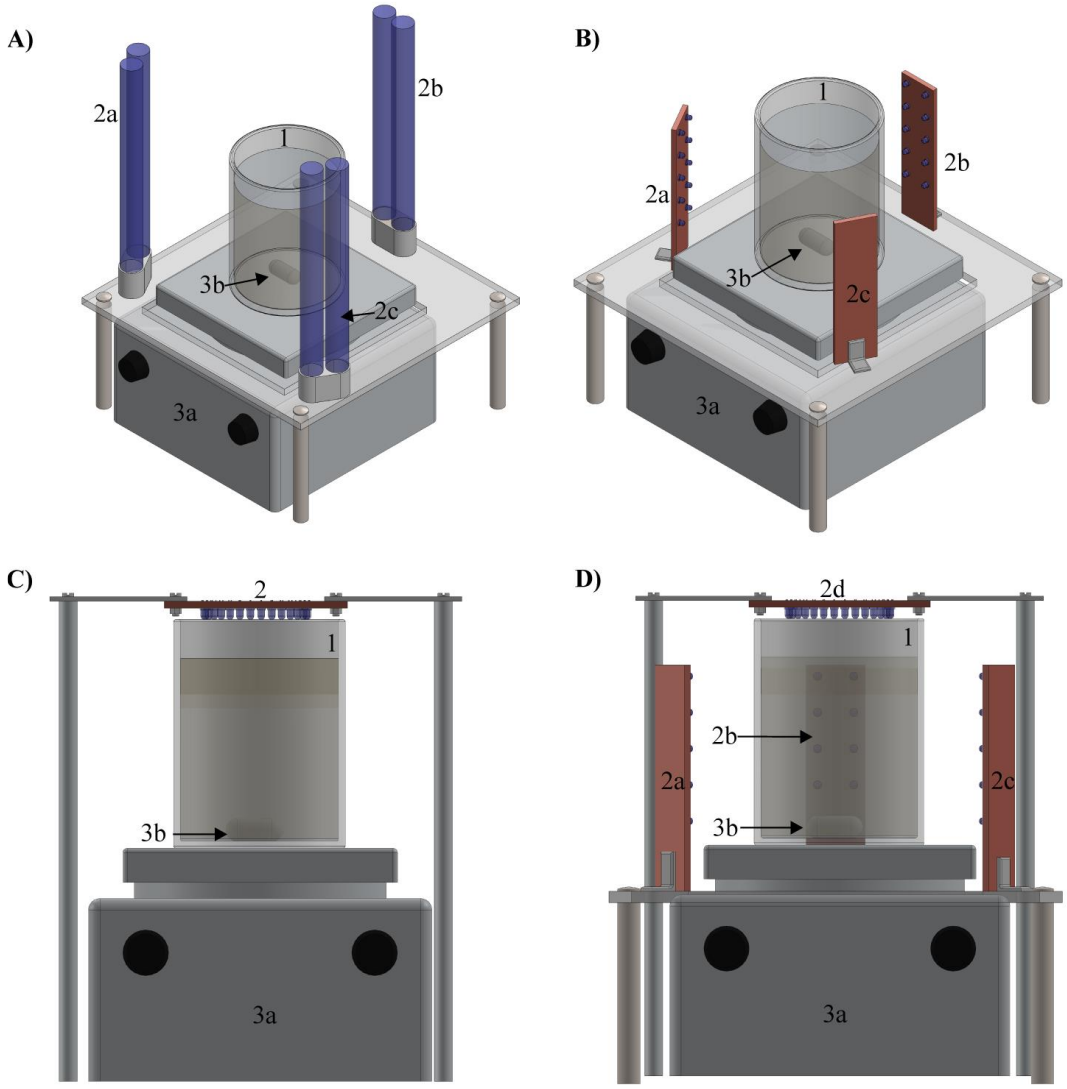

Fig. 4-1. Schematic diagram of photocatalytic reactors. **A)** UV-lamp photocatalytic reactor: 1) borosilicate vessel; 2a,b,c) UV-lamps; 3a) magnetic stirrer; 3b) magneto. **B)** Square UV-LED array photocatalytic reactor: 1) borosilicate vessel; 2a,b,c) square UV-LED arrays; 3a) magnetic stirrer; 3b) magneto. **C)** Radial UV-LED array photocatalytic reactor: 1) borosilicate vessel; 2) radial UV-LED array; 3a) magnetic stirrer; 3b) magneto. **D)** Square&radial UV-LED array photocatalytic reactor: 1) borosilicate vessel; 2a,b,c) square UV-LED arrays; 2d) radial UV-LED array; 3a) magnetic stirrer; 3b) magneto.

The decolorization rate was measured to determine the efficiency of the treatment, and was calculated by:

$$Decolorization\ (\%) = \left(\frac{Abs_0 - Abs}{Abs_0}\right) \times 100 \qquad \textbf{Eq. 4-1}$$

where, Abs_0 is the initial absorbance, and Abs is the absorbance at time t of the taken sample. The absorbance was determined with a with a UV–visible spectrophotometer (UV-2401, Shimadzu Corporation) at the maximum wavelength of the visible spectrum (λ = 487 nm).

4.2.5 Energy consumption

The power consumption of the AOPs for an experimental scenario, depends on different factors, such as the type of pollutant, type of light source, reactor configuration, among others. A quantitative comparison can be obtained in terms of Figures-of-merit, for the case of photocatalytic processes the efficiencies can be determined by means of the Figure-of-merit "Electric energy per order (E_{EO})", defined as the electric energy (kW) needed to degrade a pollutant by one order of magnitude (90%) in a unit volume of contaminated water (1 m^3) [66–68].

E_{EO} values [kWh/m^3/order] can be calculated by:

$$E_{EO} = \frac{(P)(t)(1000)}{(V)(60)(\log(C_0/C))} \qquad \textbf{Eq. 4-2}$$

where, P is the electric power (kW), t is the time (min), V is the water treated volume (L), C_0 and C are the initial and final concentrations of contaminant (mol/L).

4.3 Evaluation Results

Fig. 4-2 shows the different experimental photoreactors used in this chapter. The **Fig. 4-2A** is the reactor with 3 ultraviolet lamps, in **Fig. 4-2B** the reactor uses 3 square LED arrays presented in **Fig. 3-16A**, the **Fig. 4-2C** shows the reactor using the radial LED array of **Fig. 3-16B**, and finally the reactor in **Fig. 4-2D** use all designed LED arrays (squares and radial). The reactors presented were implemented with the characteristics mentioned in section **4.2.3**, and during its operation they were maintained only with the light source selected, blocking any other type of lighting that could affect the process.

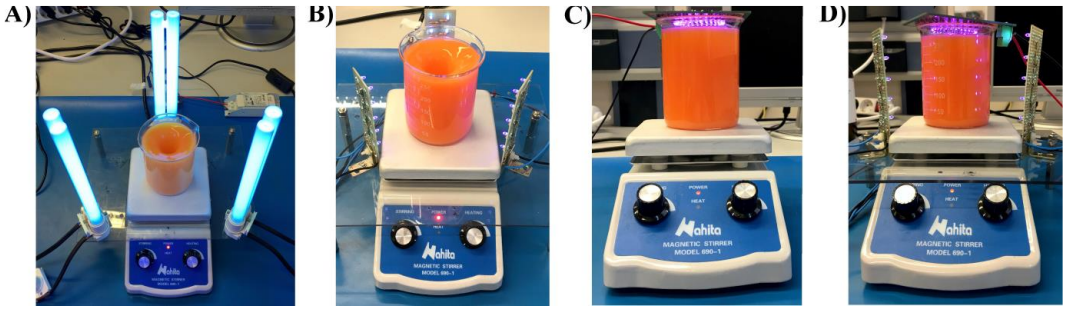

Fig. 4-2. Experimental reactors. **A)** Reactor with UV-lamps, **B)** Reactor with square LED arrays, **C)** Reactor with a radial LED array, **D)** Reactor with all UV-LEDs.

4.3.1 Photocatalytic activity

Four configurations were tested: i) The UV-lamp configuration shown in **Fig. 4-2A**; ii) A configuration using only the three square LED arrays (**Fig. 4-2B**); iii) A configuration including only the top radial distribution of LEDs (**Fig. 4-2C**), and iv) The configuration with all LEDs is shows in **Fig. 4-2D**.

With the aim to perform the comparison of the dye degradation, all the samples were prepared under the same experimental conditions. It was corroborated prior to the photodegradation that the photocatalyst does not have the ability to degrade the dye without an UV-source.

As it can be seen in **Fig. 4-3**, the performed experiments by the four analyzed configurations reached more than 90% of decolorization, which is the percentage necessary to calculate the Figure-of-merit E_{EO}.

The required time for the LED arrays configurations to reach this decolorization percentage is in all cases larger than the consumed by conventional lamps and in the last case (array with the highest number of elements) a full decolorization (100%) is achieved 20 minutes before than for the treatment with conventional lamps. In particular, it was observed that the time needed to achieve 90% decolorization was 1.74, 1.55 and 1.28 times longer than the UV lamp process for the ii), iii), and iv) UV-LED configurations respectively, and hence the geometry with more LEDs approaches more efficiently the operation of the conventional UV reactor. However, when the process is considered also in terms of energy consumption this excess

of time in the oxidation process can be compensated by the increased energetic efficiency of the process.

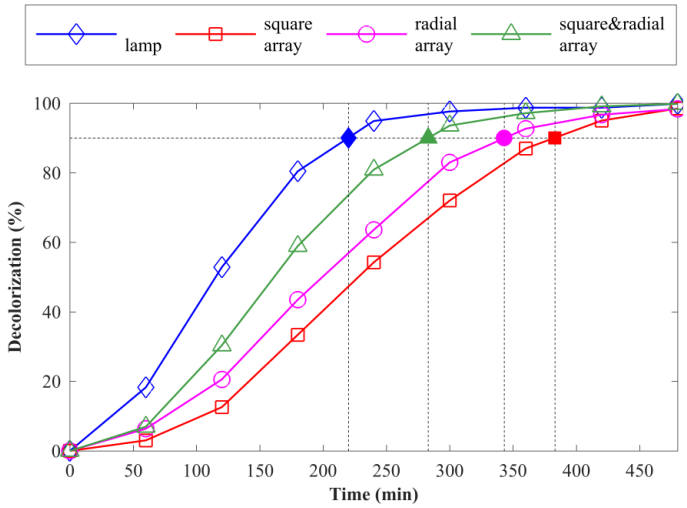

Fig. 4-3. Decolorization for the Orange PX-2R dye with different types of UV-sources, with a same initial concentration of 0. 1 g/L of dye and 1 g/L of photocatalyst.

The **Fig. 4-4** shows the evolution of the degradation of the dye made with the different UV-sources and configurations, each sample was taken every hour.

Fig. 4-4. Decolorization samples of Orange PX-2R dye with different UV-sources. **A)** lamp, **B)** square array, **C)** radial array, **D)** square&radial array.

4.3.2 Kinetic analysis

Kinetic rates obtained in the different experiments are shown in **Fig. 4-5**. As can be observed, the dye degradation in all cases follows a first-order kinetic model of Langmuir – Hinshelwood. This model provides the kinetic values (K), calculated from the slope of logarithmic absorbance values versus time of treatment, and the regression coefficients (R^2).

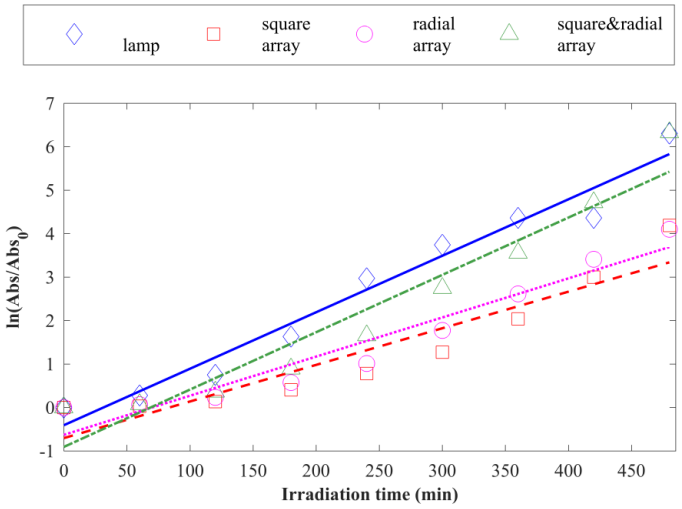

Fig. 4-5. Relation between ln(Abs/Abs$_0$) and irradiation time, with a same initial concentration of 0. 1 g/L of dye and 1 g/L of photocatalyst.

The values corresponding to the regression coefficients (R^2), as well as the kinetic degradation rate (K) are listed in **Table 4-1**. The results indicate that the rate of kinetic degradation decreases for the cases with LED lighting with fewer pieces (square and radial arrays, 30 LEDs) and the values using lamp and the array with more pieces (square&radial array, 60 LEDs) are similar.

In addition, these results suggest that exists a relationship between the lighting pattern of the source and its area of illumination. The lamp by having a wider lighting pattern covers a larger area in the reactor than the LED arrays. However, by joining the square and radial LED arrays the illuminated area of the reactor increases as well and the R^2 and K values obtained from the lamp are nearly matched.

With the aim to present in economic terms the results obtained for different ultraviolet sources and their configurations, the electrical cost of the processes was calculated. This cost was calculated considering the rate of the electric power for industrial use in Spain for the

year 2018 (0.19270 €/kWh). **Table 4-1** shows the cost of each one of the processes when reaching 90 % of the decolorization.

Table 4-1. The first-order degradation rate constant, and Costs for the decolorization of Orange PX-2R dye by different UV-sources.

UV – source	R^2	K (min^{-1})	Electrical cost (€/m^3)
Lamp	0.9664	0.0130	152.62
Square LED array	0.8764	0.0084	29.60
Radial LED array	0.9338	0.0090	26.36
Square&radial LED array	0.9341	0.0132	43.62

As can be seen in **Table 4-1**, all photocatalytic processes using LED arrays require less electrical power and are related to the number of LEDs contained in the array. However, the array with more LED elements only increases the cost by 33% than the radial LED array, and reduces the time of the photocatalytic process in one hour.

4.3.3 Energy consumption analysis

In general, the results reported in the literature rarely compare the performance between conventional lamps and LEDs, which difficult a direct comparison. Therefore, it is necessary to consider various operating parameters as the type of pollutant and its concentration, the source of illumination, the characteristics of the reactor, the photocatalyst among others. Nevertheless, the E_{EO} can enable a performance measurement with the aim to compare the efficiency in terms of energy consumption.

In order to perform the analysis of the energetic consumption with regard to the photocatalytic processes, the Figure-of-merit E_{EO} was used and 90% of degradation values were considered (**Fig. 4-3**). As it was observed in the photocatalytic activity results, decolorization by conventional ultraviolet lamps is the first to reach 90 %, however, the E_{EO} values are significantly far convenient with the use of the implemented LED arrays by means of the proposed methodology (**Table 4-2**), since conventional lamps considerably require more electrical power to carry out the photocatalytic process. According to the results, the experiments carried out with the array with the highest number of LEDs provided similar

results that those performed with the conventional UV-lamps, but reducing the energy consumption 72 %.

The **Table 4-2** shows the E_{EO} values reported in the literature to degrade different pollutant by means of advanced oxidation processes.

Table 4-2. Comparison of E_{EO} values with literature.

Source	Treatment Process	Contaminant	E_{EO} Value (kWh/m^3)	Reference
Lamp				
8 mp-lamps (8W)	Photo-Fenton	Reactive Orange 4	357.10	[69]
8 mp-lamps (8W)	Photo-Fenton	Reactive Yellow 14	416.60	[69]
1 lp-lamp (30W)	UV	Insecticide diazinon	20,000.00	[70]
8 mp-lamps (8W)	UV/H_2O_2	Reactive Orange 4	1,666.00	[69]
8 mp-lamps (8W)	UV/H_2O_2	Reactive Yellow 14	2,000.00	[69]
1 lp-lamp (30W)	UV/ZnO (14 nm)	Insecticide diazinon	1,075.30	[70]
1 lp-lamp (30W)	UV/ZnO (33 nm)	Insecticide diazinon	1,388.80	[70]
1 mp-lamp (150W)	UV/TiO_2	SDBS	595.00	[71]
8 mp-lamps (8W)	UV/TiO_2	Reactive Orange 4	500.00	[69]
8 mp-lamps (8W)	UV/TiO_2	Reactive Yellow14	344.80	[69]
3 lp-lamp (18W)	UV/TiO_2	Orange PX-2R	628.14	[*]
LED				
30 LEDs (385nm)	UV/TiO_2	Orange PX-2R	129.45	[*]
30 LEDs (385nm)	UV/TiO_2	Orange PX-2R	119.04	[*]
60 LEDs (385nm)	UV/TiO_2	Orange PX-2R	178.12	[*]
96 LEDs (375nm)	UV/TiO_2	Reactive Black 5	220.00	[29]
15 LEDs (390-410nm)	UV/TiO_2	Malachite Green	789.47	[51]
15 LEDs (390-410nm)	UV/TiO_2	Methylene Blue	3000.00	[51]
15 LEDs (390-410nm)	UV/TiO_2	Rhodamine B	1500.00	[51]
384 LEDs (395nm)	UV/TiO_2	O-cresol	37.00	[57]
180 LEDs (375-380nm)	UV/TiO_2	SDBS	640.00	[71]
4 LEDs (390-410nm)	UV/TNA-300	Congo red	228.00	[49]
4 LEDs (390-410nm)	UV/TNA-500	Congo red	317.00	[49]
4 LEDs (390-410nm)	UV	Congo red	14,285.00	[49]
6 LEDs (360nm)	UV/Peroxydisulfate	Basic Red 46	155.40	[72]

[*] experimental results for this chapter

For the case of the UV-LED/TiO_2/dye processes two tendencies are manifested, i) implementations with more LEDs than the arrays proposed in this chapter and ii) implementations with fewer elements of LEDs. For both cases, the arrays generated by this methodology require a lesser amount of electrical power. For i) the amount of electric energy decreases about 20 – 45 %, and for ii) the electric energy consumed by the optimized arrays only requires between 5 – 15 % of the total energy by other arrays, depending on the type of array chosen (30 or 60 LEDs) for both cases.

As for the experimental scenarios proposed in this chapter, it can be noticed that the optimized LED arrays only require between 10 – 28 % of the energy consumed by ultraviolet lamps to decolorate the same amount of water, the E_{EO} value of this photoreactor indicates an energy saving since with the same amount of energy it is possible to decolorize an amount of 3.5 times more water than conventional lamps.

It can be observed that in general the use of LEDs reduces the energy consumption of the treatment in comparison to the use of conventional UV-lamps. However, it is important to highlight that in some cases the consumption obtained is equals or even higher. This could be attributed to the fact that the distribution of the LEDs was not optimized during the treatment.

4.4 Discussion and conclusions

Photonics technology is present nowadays in a vast number of applications where the selection of the proper light source plays a crucial role for the implementation and optimization of practical devices. Light sources have evolved during the last decade and the efficient use of energy is an imperative requirement in modern lighting technologies for their use in medical, chemical and environmental applications. In order to exploit these advantages, it was necessary to study methods that fulfilled the best characteristics of the lighting sources that could replace to the conventional ones, thus in this chapter uniform irradiance models were applied with the aim to create a methodology for calculating optimized LED arrays, taking into account the photochemical requirements of the photocatalytic reactor, and demonstrating the feasibility of the method for the degradation of textile dyes.

As is noted, the use of conventional lamps leads to an inefficiency of the photocatalytic process, since the photocatalyst does not take advantage of all the energy emitted by the

lamp, which produces an overconsumption of energy or the need to modifying the chemical characteristics of the photocatalyst, increasing the cost of the process. The use of LEDs could help to reduce the necessary energy to carry out the photocatalysis process (with the implicit benefits of the LED sources as lifetime, avoiding the use of mercury lighting sources), but if the LED arrays are not carefully optimized the reduction in electricity consumption cannot be assured, and the adding LEDs could counterproductively increase the cost of the process (as well as the cost of the implementation), thus, an improvement in photocatalytic results is not guaranteed. In this chapter, by emphasizing the minimum number of elements as well as their optimal distribution for the LED arrays with regard to the physical dimensions of the reactor, the obtained results show that a diminishing on the energy consumption for the photocatalytic process up to 90% can be achieved.

In this chapter we can see, that the optimally increasing the LED elements from 30 to 60 is compensated by the decrease in the time of decolorization, as well as by an low energy consumption (119.45 vs 178.12 kWh/m^3/order respectively), reaching a 100% of the decolorization before using lamps (416 vs 435 min).

Chapter 5. WAVELENGTH ANALYSIS

5.1 Introduction

Temperature is an important parameter in photocatalytic processes and sources of illumination. Photocatalytic processes work optimally at room temperature[32,73], nevertheless, LED lightning sources may affect the emission spectrum when there are significant temperature changes, this movement [74,75].

Most LEDs are made of GaAs and have direct energy gap semiconductors, on forward biasing the LED excess electron hole pairs are recombined with each other's producing photons of light which are emitted to outside of the diode. The emitted light intensity is proportional to the excess charges which increases linearly with the diode current, because, increasing the temperature, the band gap energy decreases and emitted wavelength increases[76,77].

Since the temperature affects the wavelength emitted by the LEDs, in this chapter, the wavelength shift of the LED was verified, as well as the existence of a significant change in photocatalytic processes when the LED light source undergoes temperature variations.

5.2 Evaluation tests

Two cases were corroborate: a) A cooling device was implemented in a LED385-33 in order to move the emission peak to a lower wavelength. b) Once the wavelength shift was measured, the same cooling device was implemented in the Radial LED array with the aim to corroborate the existence of a variation in the performance of the photocatalytic process in the presence of a change in the wavelength and intensity of the LEDs.

5.3 Evaluation Results

As seen in **Fig. 5-1**, the wavelength shift of LED385-33 when cooled to -7 ° C was 1.76 nm, changed from 384.35 to 382.59 nm, and its intensity increased 1.7 mW, nevertheless, to generate these changes were applied 2 A of power.

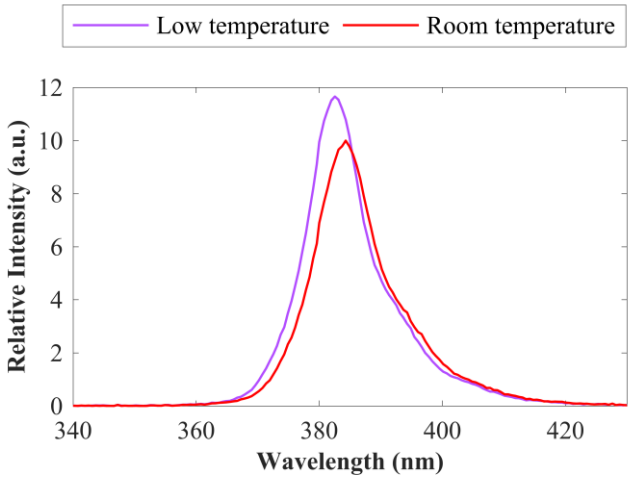

Fig. 5-1. Wavelength shift of the UV-source LED385-33

After measuring the wavelength shift and the intensity increase, the decolorization of the Orange PX-2R dye was performed by cooling the radial LED array to -7 ° C.

Fig. 5-2 shows the decolorization curve obtained after cooling the UV-LED source compared to the uncooling decolorization curve. The results show that there is a variation in performance, nonetheless, it can be negligible since there is no improvement in process time or efficiency, besides, to cool the array requires 2 A of power.

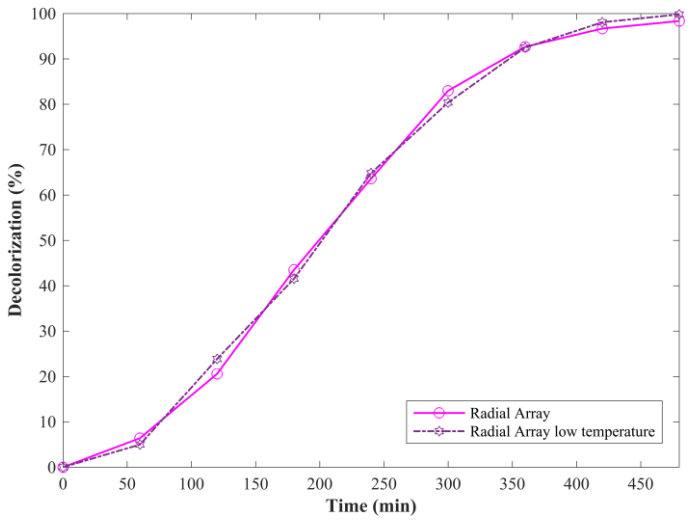

Fig. 5-2. Orange PX-2R dye decolorization with different temperature.

5.4 Discussion and conclusions

Although TiO_2 has a wide working area in the ultraviolet zone (400 – 488 nm), shifting the emission peak from 384.35 to 382.59 (1.76 nm) and increasing its intensity does not generate a significant change in the Photocatalytic process performance.

While the LEDs can work at -20 C, the manufacturer does not recommend low temperatures for long periods of time, since the life of the diode could be shortened.

To cause a significant improvement in the performance of the photocatalytic process, it would probably be necessary to cool the array evenly at -15 ° C, however, it would increase energy consumption to decrease the temperature, which is not recommended in the optimization of this processes.

Chapter 6. In-situ Monitoring of Decolorization of Textile Dyes

6.1 Introduction

Water pollution is nowadays one of the most worrying health problems influencing the life of all living beings and textile industry, among the sectors with larger influence in the production of wastewater[7,8,78], uses more than 100,000 different dyes, with roughly 280,000 tons lost in the textile effluents every year[9,10]. Textile wastewater is commonly contaminated with high concentrations of organic substances derived from various residues of dyes and different chemical additives [8,9]. Approximately 800,000 tons are synthetic azo dyes, widely used because of their high reactivity and color resilience [6,7,8]. For their mineralization and degradation advanced oxidation processes are commonly used [20–22]. Amongst the AOPs, photocatalytic process is highlighted due to their high efficiency in the removal of contaminants, including synthetic dyes [30,79].

Current photocatalytic processes in aqueous solution involve different types of reactors [52,80–88], which can be classified in different groups according to their geometry (e.g. tubular or cylindrical, rectangular or square reactors among others), liquid agitation techniques (e.g. continuous flow reactors, stirrer rotation for instance) and lightning source including mainly low or medium pressure ultraviolet lamps [42,89–92], currently being replaced by LED lighting [51,55,93–97], which can reduce the size of the reactors allowing to make compact photo reactors known as mini reactors or micro reactors [49,98,99]. These reactors usually work with less than 1 Liter of water [29,31,49,50,96–101], using photocatalysts either in suspension [31,101–104] or immobilized [105–107]. Reactors with photocatalyst in suspension are the mostly used, since it is not necessary to obtain any previous treatment of the photocatalyst. On the other hand, reactors with immobilized photocatalyst, used for diverse applications such as continuous flow processes, need a careful preparation to avoid low reaction rates [106].

Monitoring of the degree of oxidation achieved in AOPs is a crucial parameter to determine when the process is completed (i.e. measurement Chemical Oxygen Demand (COD), Total Organic Carbon (TOC), Biochemical Oxygen Demand (BOD))[31,42,90,100].

In particular, for dyed solutions the principal measurement of the degree of decolorization is used[4,11,14,108,109]. This analysis involves frequently a measurement of the absorbance at different times obtained by extracting samples periodically, generating a decrease in the water volume (non-negligible in such mini reactors) and altering the photocatalysts concentration [31,101]. An improvement of the existing monitoring techniques should revert in as more efficient control of the oxidation process. In particular, online monitoring could offer a solution conserving the volume and catalyst concentration of the treated water. This possibility has been currently proposed for monitoring in reactors with immobilized photocatalyst[95,98,110,111], but not for photocatalyst in suspension due to its intrinsic large scattering[32,39,41,112–115].

In this chapter we propose a novel implementation for the online monitoring of dye decolorization in photocatalytic in suspension reactors, which can be adapted to different reactor geometries, taking profit of the natural process of scattering to measure the color removal. The frequency spectrum of the scattered radiation when the solution is illuminated by a white-light source is continuously monitored by a fiber-coupled spectrometer measuring the degree of decolorization in real time.

6.2 Methodology

6.2.1 Reagents

The materials used for this experiments were six different textile dyes of the azo chromophore group (**Table 6-1**), Orange PX-2R dye (CAS No. 12225-85-3), Procion Blue H-EXL (CAS No. 124448-55-1), Procion Navy H-EXL (mixed of CAS No. 186554-26-7 and CAS No. 186554-17-8), Procion Crimson H-EXL (CAS No. 186554-26-7), Remazol Black B133 (CAS No. 17095-24-8), and Procion Yellow H-EXL (mixed of CAS No. 72906-24-2 and CAS No. 72906-25-3), and titanium dioxide powder (TiO_2) from the Sigma-Aldrich manufacturer (CAS number 13463-67-7), with particles of 21 nm, surface area of 35 – 65 m^2 /g and a molecular weight 78.87 g/mol.

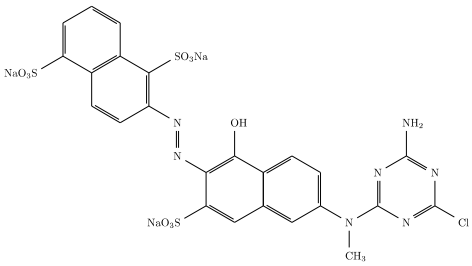

Fig. 6-1. Chemical structure CAS No. 12225-85-3.

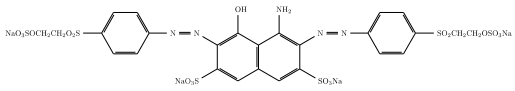

Fig. 6-2. Chemical structure CAS No. 17095-24-8.

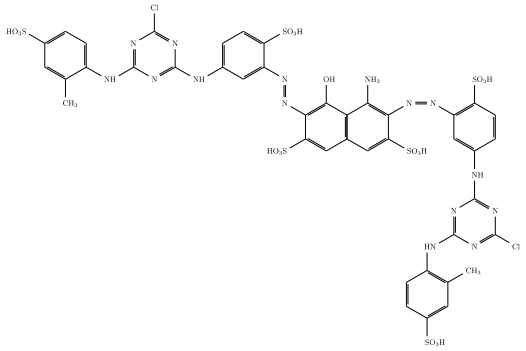

Fig. 6-3. Chemical structure CAS No. 186554-27-8.

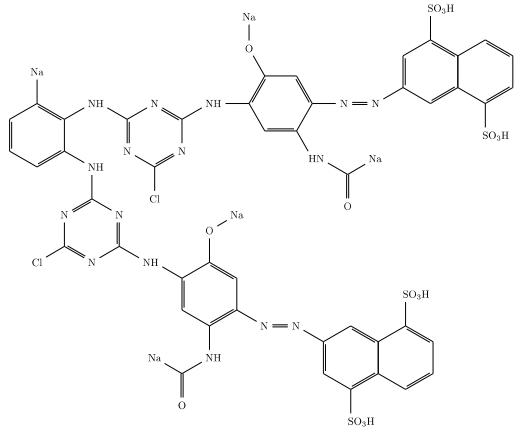

Fig. 6-4. Chemical structure CAS No. 72916-24-2.

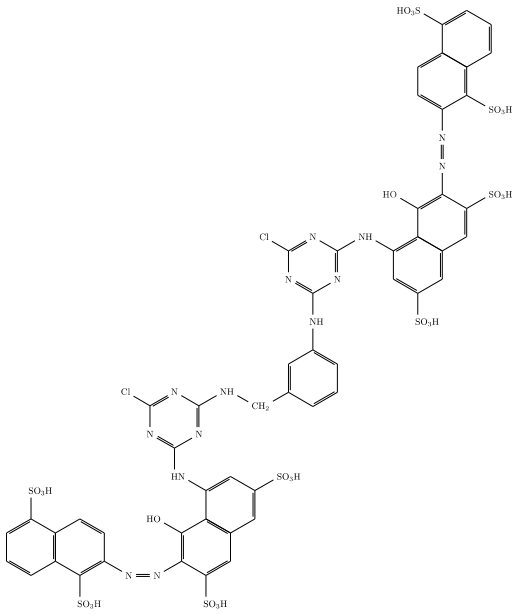

Fig. 6-5. Chemical structure CAS No. 186554-26-7.

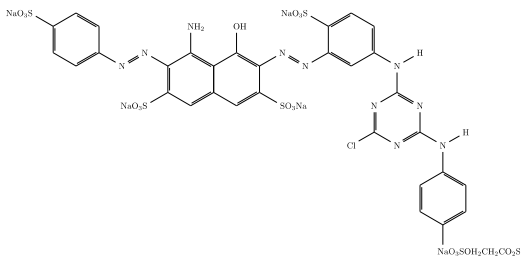

Fig. 6-6. Chemical structure CAS No. 124448-55-1.

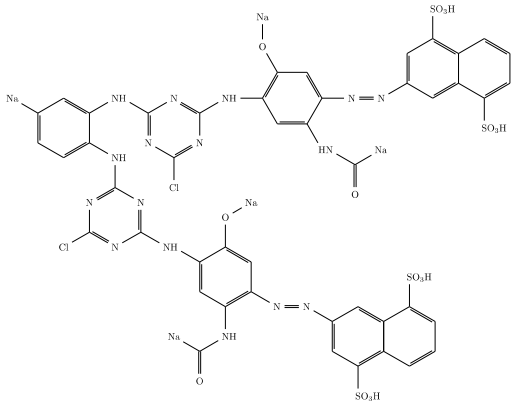

Fig. 6-7. Chemical structure CAS No. 72906-25-3.

Table 6-1. Description of the selected dyes.

Abbr. Name	Commercial Name	C. I. Name	Num. Reactive Groups	λ_{max}	Fig.
OP2	Orange PX-2R	Reactive Orange 13	1	487 nm	**Fig. 6-1**
RB	Remazol Black B133	Reactive Black 5	2	598 nm	**Fig. 6-2**
PC	Procion Crimson H-EXL	Reactive Red 231	2	545 nm	**Fig. 6-5**
PN	Procion Navy H-EXL	Not registered	2	606 nm	**Fig. 6-3**
PB	Procion Blue H-EXL	Reactive Blue 198	2	624 nm	**Fig. 6-6**
PY	Procion Yellow H-EXL	Reactive Yellow 138:1	2	416 nm	**Fig. 6-4** and **Fig. 6-7**

6.2.2 Decolorization experiments

For the measurements of the decolorization a photocatalytic reactor was built using a 250 mL borosilicate vessel and a magnetic stirrer. ¡Error! No se encuentra el origen de la referencia.**A** shows schematic diagram of the photoreactor with the in-situ monitoring configuration, ¡Error! No se encuentra el origen de la referencia.**B** shows the schematic diagram of the effect of the scattering in a photoreactor with suspended catalyst, the reactor has two square UV-LED arrays (UV-LED array (2) and(4)), placed 120º around the container, at a distance of 8 cm from the center of the reactor, and another three non-uniform UV-LED arrays placed 120º around the vessel (UV-LED array (1), (3) and (5)), at a distance of 4 cm from the center of the reactor, and UV-LED radial array, placed in the upper part of the photoreactor, at a distance of 10 cm with respect to the bottom of the vessel.

The geometric configuration and the separation between UV-LEDs was selected with the aim to obtain an illumination as uniform as possible in the reactor using uniform irradiance models[96]. The UV-LEDs were manufactured by Roithner LaserTechnik LED385-33 UVA, with peak wavelength at 385 nm, radiated power of 11 mW and power dissipation of 200 mW.

6.2.3 Monitoring with recirculation system

In a first attempt to achieve this goal the geometry of the initial photoreactor (see **Fig. 6-8A**) was modified including a pump to circulate the dye solution into an external circuit and using 1 mm thick cuvette to measure the degree of decolorization of the sample (see **Fig. 6-8B**).

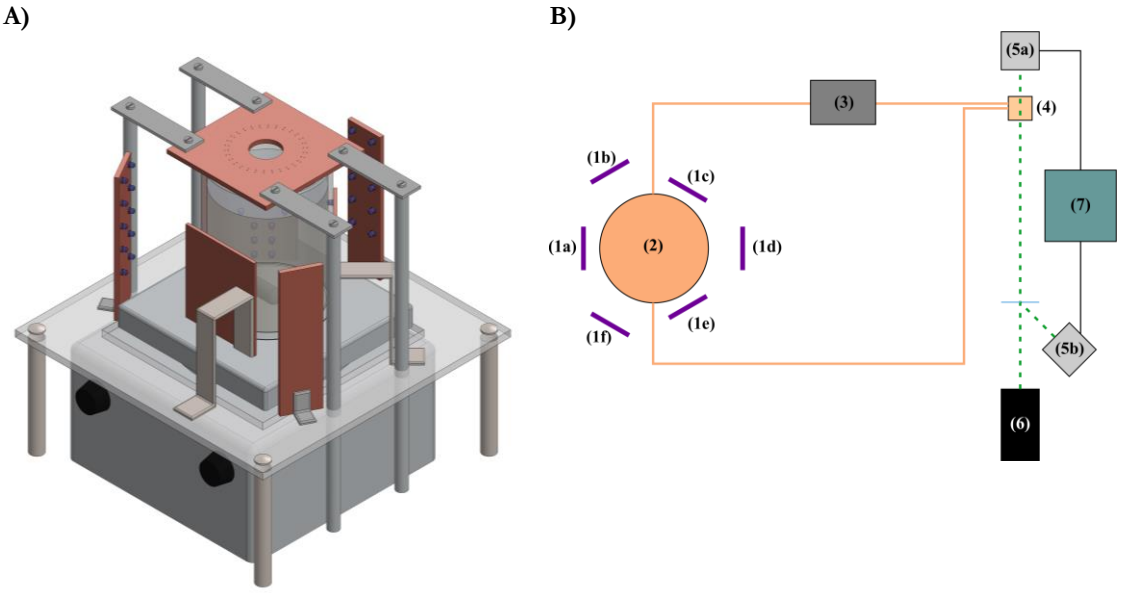

Fig. 6-8. Schematic diagrams. **A)** Reactor with placement of all UV-LED arrays. **B)** Diagram of monitoring with recirculation system, (1a-f) UV-LED arrays, (2) Photoreactor, (3) Pump, (4) Cuvette for sample analysis, (5a-b) Photodetector, (6) Laser, (7) Data Acquisition System.

6.2.4 Online monitoring

The online monitoring configuration used a white-light lamp (Thorlabs OSL1-EC), whose irradiance is emitted in a spectral range different from the photocatalyst activation zone (<388 nm) to avoid the alteration of the photocatalytic process, this lamp was placed normal to the reactor's surface, illuminating in the radial direction to induce the scattering from the catalyst in suspension. Also, a fiber bundle connected to an spectrometer (Andor Shamrock 303i) was oriented in order to collect the scattered radiation from the reactor, but avoiding direct ultraviolet light from the UV sources of the photocatalytic process, in addition between the reference lamp and the spectrometer a barrier was placed to avoid erroneous readings.

The spectrometer was configured to take a sample every 5 minutes until the total decolorization of each dye was reached.

The transmittance was calculated by:

$$\%T = \left(\frac{I}{I_0}\right) \times 100 \qquad \textbf{Eq. 6-1}$$

where I is the transmitted light intensity, and I_0 is the original light intensity.

Absorbance can be calculated given its relation to transmittance by:

$$A = 2 - log(\%T) \qquad \textbf{Eq. 6-2}$$

where %T is the transmittance as a percentage.

The percentage of decolorization was calculated by **Eq. 4-1**.

6.2.5 Measurements with traditional method

With the aim to measure the absorbance value by the traditional method it is necessary to take a sample, and remove the titanium dioxide (e.g. filtration, centrifugation) to be able to use the spectrophotometer (UV-2401, Shimadzu Corporation) at the maximum wavelength of the visible spectrum of each dye (**Table 6-1**). Subsequently, the percentage of decolorization can be calculated by **¡Error! No se encuentra el origen de la referencia.**.

6.2.6 Photocatalytic decolorization experiments

In order to simulate the effluents after the dyeing process, 250 mL of distilled water were mixed with 0.1 g/L of each dye. Before photodegradation, the solution was mixed with 1 g/L of photocatalyst in suspension and then the mixture was put on magnetic stirrer in complete darkness for 30 minutes to ensure the adsorption of the dye on the surface of the catalyst. After 30 minutes, the UV-LED source was turned on with the mixture in constant agitation. The catalytic process was carried out until the total color removal of each dye was reached. Initial and final traditional samples of each dye were taken to verify the decolorization values obtained with online monitoring against the traditional method.

6.3 Evaluation results

6.3.1 Monitoring with recirculation system

Fig. 6-9 shows the photoreactor with the recirculation system implemented, this configuration presented some problems, in the circulation process part of the catalyst was adsorbed at the circuit walls and the cuvette, it was also not possible to make a direct measure through the cuvette in transmission due to the high scattering present.

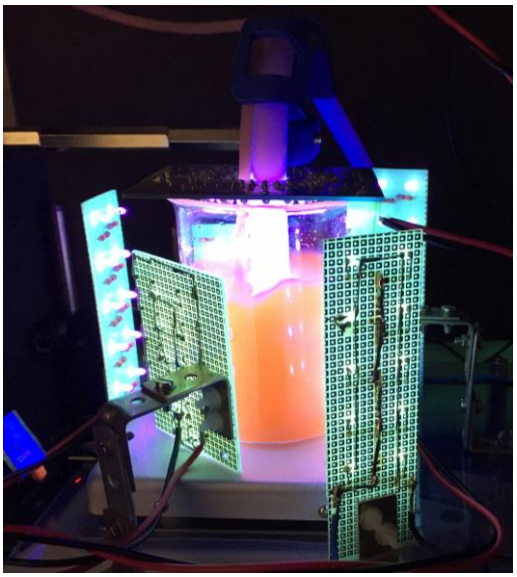

Fig. 6-9. Implemented reactor with recirculation system.

Fig. 6-10 shows the cuvette used for decolorization analysis. As can be seen in **Fig. 6-10A** due to the scattering of the cuvette the reference Laser could not cross the sample to analyze it with the photodetector, and in **Fig. 6-10B** can be see the photocatalyst stuck in the cuvette corners.

In another attempt to transmit the light through the cuvette, the reference Laser was substituted for a white light lamp, however, as can be seen in **Fig. 6-10C** there is a large amount of scattering that inhibits correct measurement.

Using immobilized TiO_2 geometries can palliate the effect of the scattering but can introduce other problems such as how to obtain a uniform illumination of the sample (this is a crucial aspect in photocatalytic processes).

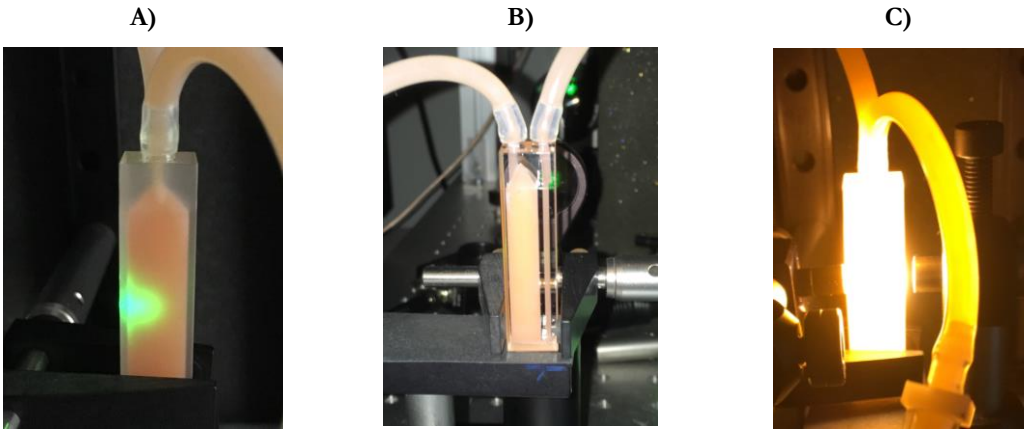

Fig. 6-10. Cuvette for sample analysis. **A)** Lateral view, **B)** Front view, **C)** Lateral view with white lamp illumination.

6.3.2 Online monitoring

In the experiments a photocatalytic microreactor with suspended TiO_2 photocatalyst was used. The titanium dioxide spherical nanoparticles, are suspended in water and continuously stirred to avoid precipitation of the suspension. As a consequence the averaged particle density and hence the averaged index of refraction at each microscopic volume element of the suspension will show temporal fluctuations, leading to a quite uniform scattering distribution in all directions when illuminated by a light beam. The size of the scattering centers, much smaller than the wavelength, leads to Rayleigh-type scattering with omnidirectional dispersion acting quite effectively in the visible part of the spectrum.

The conventional method to determine the decolorization degree requires filtering the suspended photocatalyst to measure the absorbance using a spectrophotometer. The degree of decolorization is directly related to the amount of oxidation achieved in the sample.

Online monitoring of the decolorization process would allow to follow the kinetics of the process in real time.

We propose a new solution taking profit of the natural scattering emitted over broad spectral regions with the aim to perform an online monitoring of the spectrum directly from the reactor body. We will also demonstrate its performance in the monitoring of the decolorization of azo dyes.

Fig. 6-11 shows the implemented photoreactor with the elements to perform online monitoring, this reactor uses 86 LEDs, distributed in different arrays for the photocatalytic

process and was implemented according to the description in **¡Error! No se encuentra el origen de la referencia.A**.

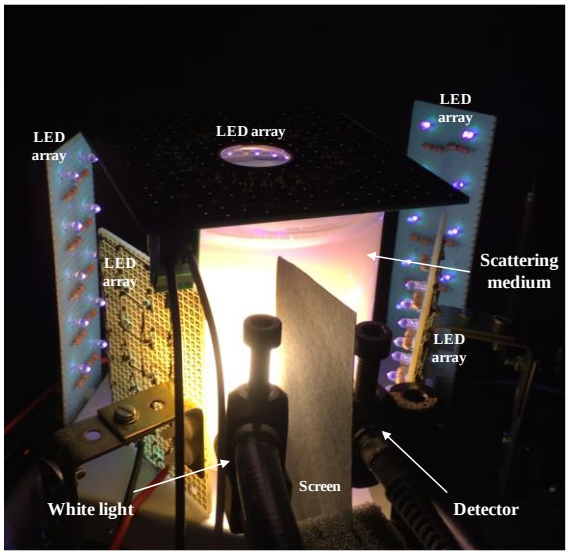

Fig. 6-11. Implemented photocatalytic reactor with decolorization monitoring.

For the monitoring we used a white light source coupled to a fiber bundle and placed close to the reactor wall illuminating the dye solution. In the **Fig. 6-11** it can be seen the strong scattering present in the illuminated solution. The scattered radiation is captured by a second fiber bundle and coupled to a spectrometer to record its frequency spectrum. Since the scattering of radiation is omnidirectional, the detection fiber bundle can be placed in any location adequate to the geometry of the reactor. In the experiments the fiber bundle was placed close to the source using a screen in order to eliminate direct coupling from the source to the detector. The acquisition process can be automatized allowing the recording of the spectrum of the dye at selected times. In each experiment measures were taken every 5 minutes automatically.

As initial reference the spectrum of clean deionized water with an amount of photocatalyst in suspension identical to that used in the dye samples and with identical magnetic stirring conditions was recorded. The capabilities of this system were tested by monitoring the decolorization process of six different dyes with colors varying along the visible spectrum (details of the dyes used are presented in **Table 6-1**). **Fig. 6-12** shows the intensity spectral curves, recorded for each sample. The arrows indicate the direction of change of the spectra as a function of time, indicating that the intensity of the spectrum signal recorded increases with time as the decolorization process takes place. For these measurements a calibrated optical illumination to obtain absolute values of irradiance is not needed, since merely the

relative variations of the spectrum are considered. From these curves an increase of the transparency of the samples, given by the increase of the overall spectrum intensity, can be inferred.

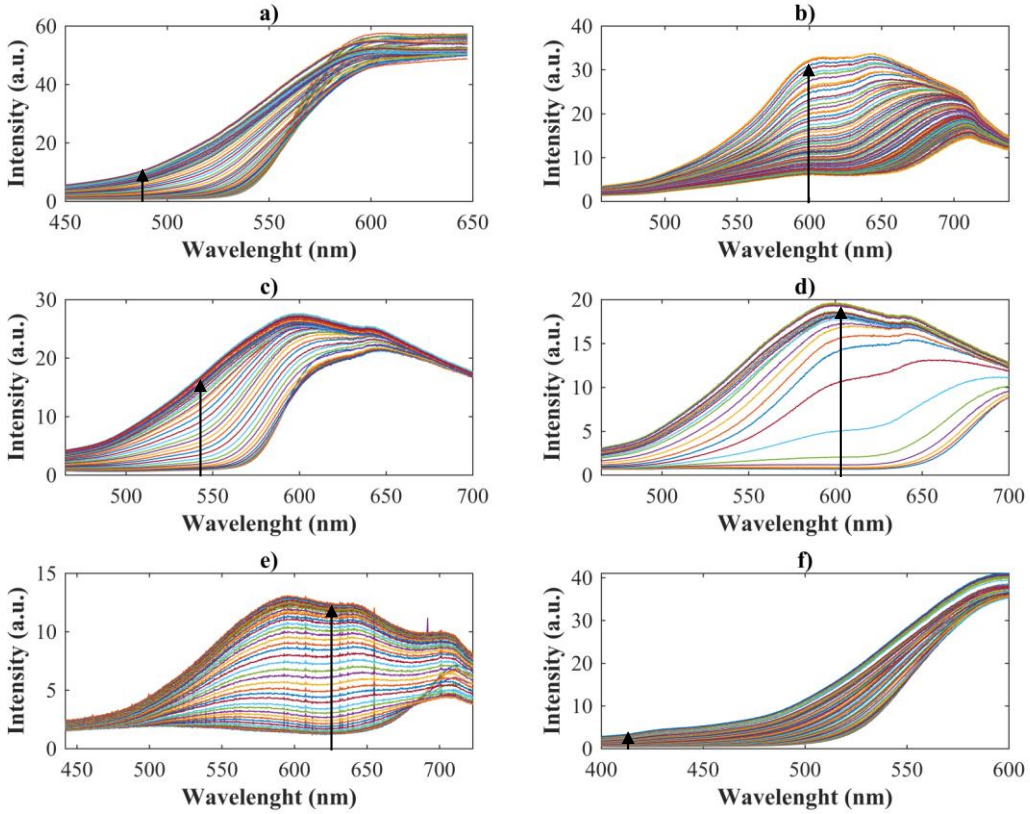

Fig. 6-12. Spectrum recorded of each dye as a function of time. **a)** OP2, **b)** RB, **c)** PC, **d)** PN, **e)** PB, **f)** PY.

Taking as a reference the spectrum of the TiO_2 suspension in deionized water, normalized values of the transmittance of the dye during the oxidation process are shown in **Fig. 6-13**. These curves allow to determine also which wavelengths are more sensitive to the decolorization process according to the characteristics of the dye.

Taking as a reference the spectrum of the TiO_2 suspension in deionized water, normalized values of the transmittance of the dye during the oxidation process are shown in **Fig. 6-13**. These curves allow to determine also which wavelengths are more sensitive to the decolorization process according to the characteristics of the dye.

Fig. 6-14 shows a measure of the normalized absorbance of the sample, obtained from the recorded spectra using **Eq. 6-2**. The absorbance values decrease when the color is removed from the dyed water.

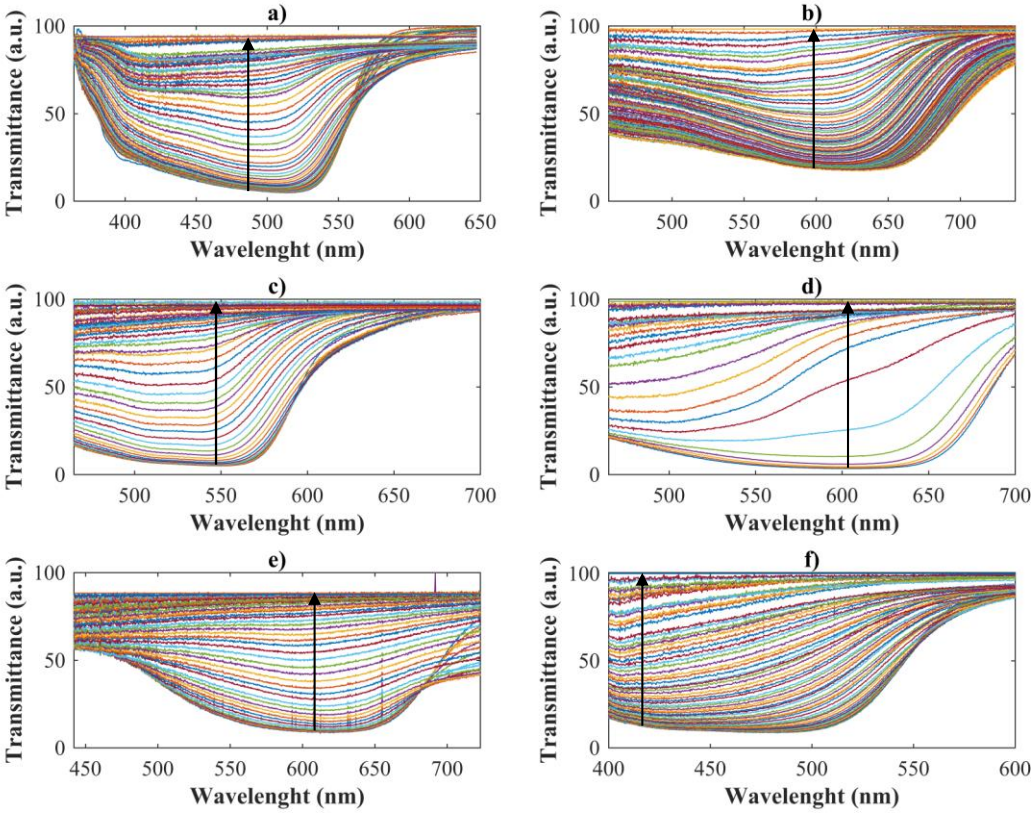

Fig. 6-13. Transmittance of each dye. **a)** OP2, **b)** b **c)** PC, **d)** PN, **e)** PB, **f)** PY.

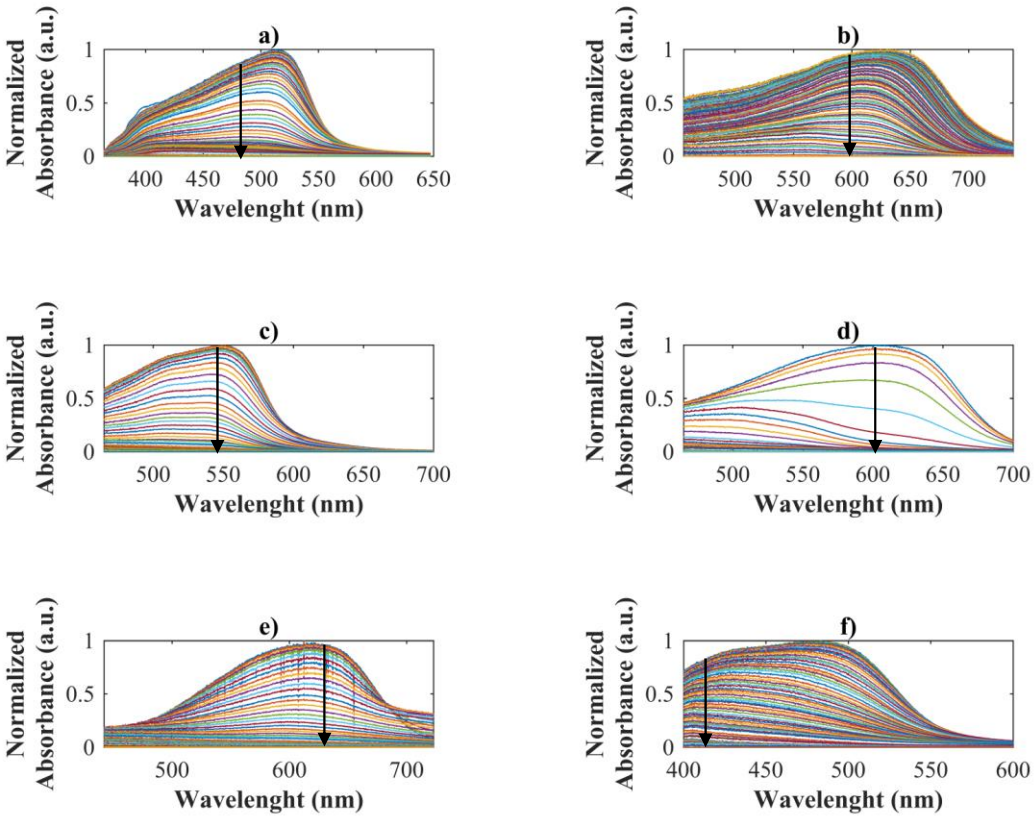

Fig. 6-14. Absorbance of each dye. **a)** OP2, **b)** RB, **c)** PC, **d)** PN, **e)** PB, **f)** PY.

The decolorization percentages, calculated using the **¡Error! No se encuentra el origen de la referencia.** using the maximum absorbance of each dye (information of **Table 6-1**) allow to extract kinetic information of the oxidation process as show in **Fig. 6-15**. These figures show that in all cases 100% of decolorization was reached with varying oxidation velocities depending of the nature of each dye.

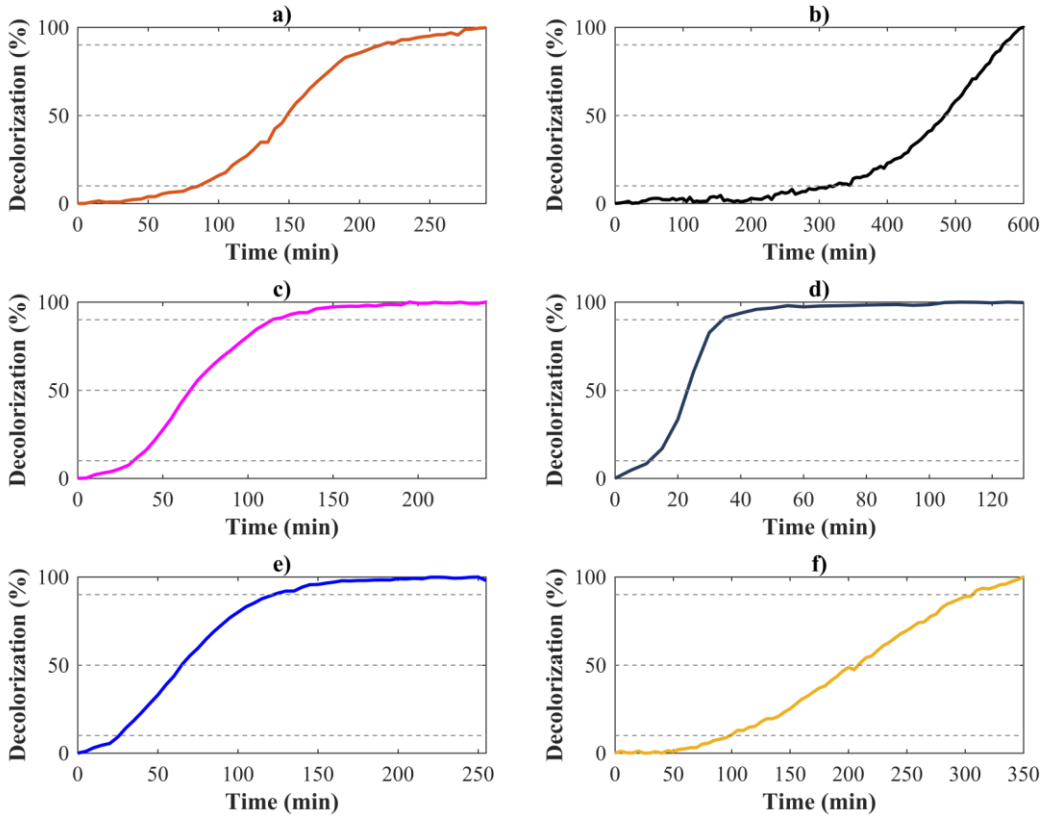

Fig. 6-15. Decolorization of each dye. **a)** OP2, **b)** RB, **c)** PC, **d)** PN, **e)** PB, **f)** PY.

Fig. 6-16 shows the initial and final decolorization samples of each dye by the in-situ monitoring.

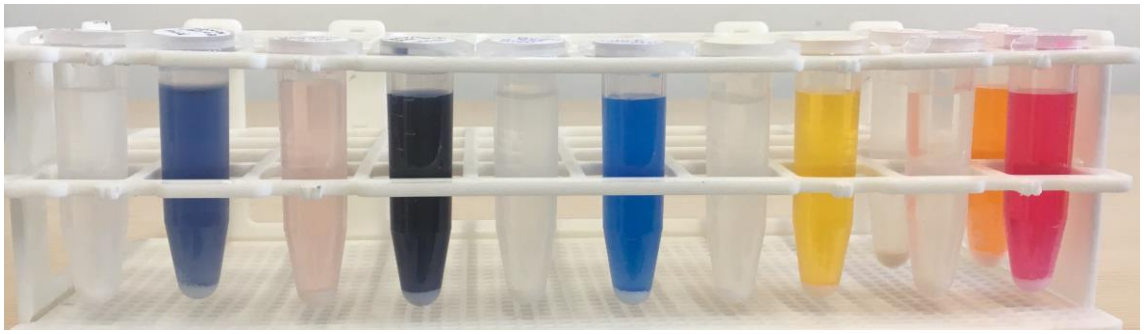

Fig. 6-16. Decolorization samples initial and final of each dye.

The total decolorization time for each one of the tested dyes is shown in **Fig. 6-17** ranging between the 2 hours and 10 hours. The online measurement allowed to make a completely automatized recording.

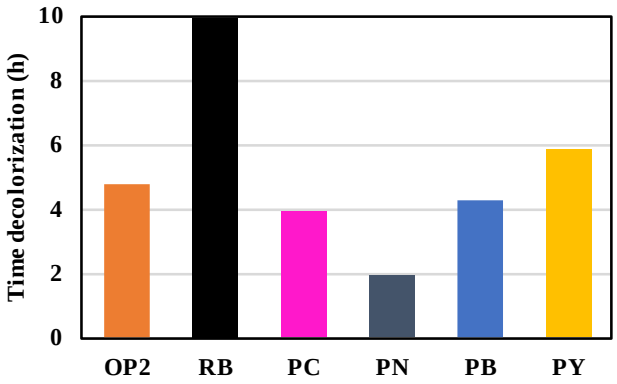

Fig. 6-17. Time of decolorization of each dye.

6.3.3 Measured absorbance with traditional method

With the aim to compare the results obtained in this in-situ monitoring with the traditional method employed, initial and final samples of each of the photocatalytic processes (each dye) were analyzed. The absorbance values were measured using a 1/20 dilution after centrifugation to remove the titanium dioxide in suspension. The absorbance curves obtained (initial and final), plotted in **Fig. 6-18**, show equivalent trends to those obtained by the in-situ method.

6.3.4 Kinetic values and Energy consumption

The dyes degradation rate at each experiment follows a first-order kinetic model of Langmuir – Hinshelwood, this model provides the kinetic values (K), calculated from the slope of logarithmic absorbance values versus time of treatment, and the regression coefficients (R^2). In **Table 6-2** the values corresponding to the regression coefficients (R^2), and the kinetic degradation rate (K) are listed. Moreover, since each decolorization process had a different duration, the calculation of the energy consumption is also listed in the table. When the degradation rate of the Orange PX-2R dye is calculated using the traditional method, the values of R^2, K obtained are 0.9341 and 0.0132 respectively, which are close to the values of the online monitoring.

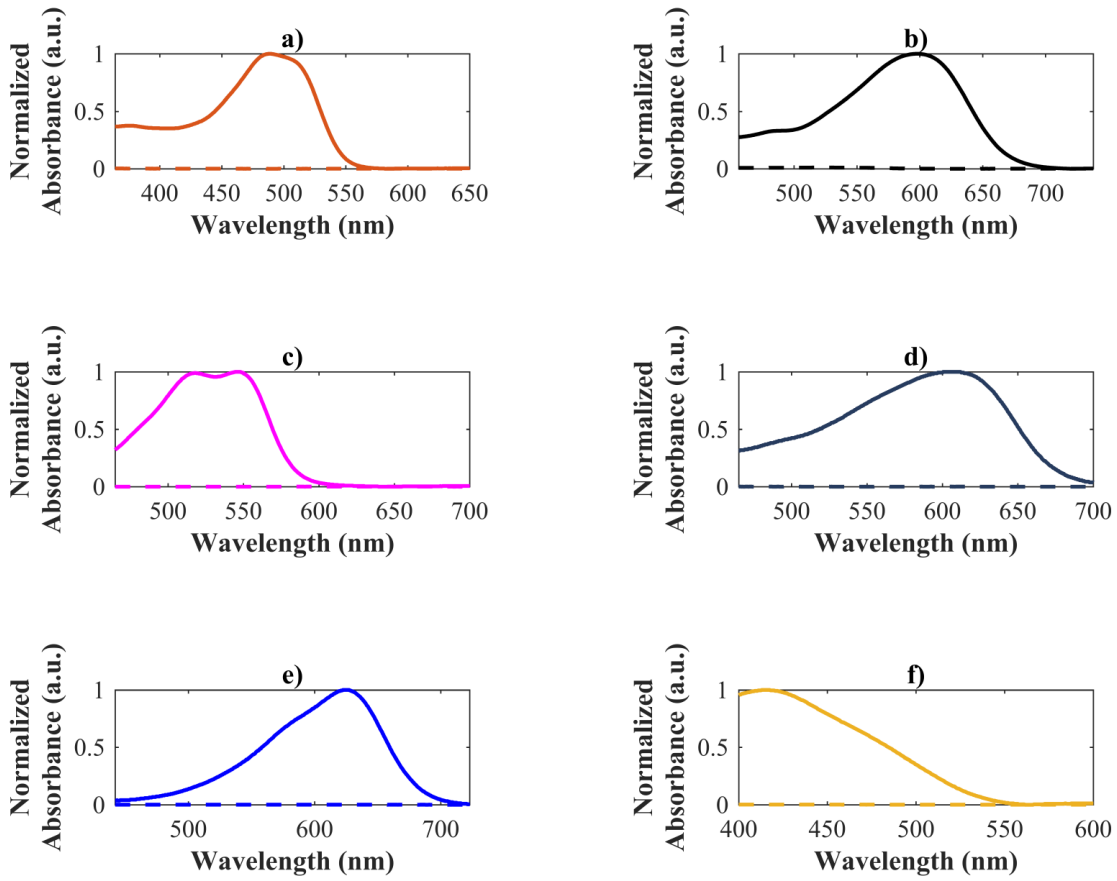

Fig. 6-18. Absorbance of each dye by traditional method. **a)** OP2, **b)** RB, **c)** PC, **d)** PN, **e)** PB, **f)** PY.

Table 6-2. First-order degradation rate constant, and Energy Consumption for the decolorization of azo dyes.

Dye	R^2	K (min^{-1})	Energy Consumption (kWh/m^3)
Orange PX-2R	0.9232	0.0159	332.53
Remazol Black B133	0.7218	0.0101	688.00
Procion Crimson H-EXL	0.9060	0.0281	269.47
Procion Navy H-EXL	0.9861	0.0232	131.87
Procion Blue H-EXL	0.7610	0.0131	292.40
Procion Yellow H-EXL	0.7870	0.0219	407.07

6.4 Discussion and conclusions

The implementation of this online monitoring technique has been developed as an alternative method to the traditional decolorization analysis schemes based on photocatalytic processes.

In this work, it was proved that the scattering produced by suspended titanium dioxide, can be exploited in order to perform the online monitoring of color removal of azo dyes in photocatalytic processes. Thus avoiding, alterations or interruptions during the process by maintaining unaltered the photocatalyst concentration, as well as the volume of the contaminant (crucial condition in minireactors and microreactors).

Since the scattering is present due to the fluctuations in the suspended particles density, this the technique could be extended to other semiconductor photocatalysts with different index of refraction or particle dimensions.

In addition, since this technique allows to arbitrarily select the sampling frequency of the acquired spectra, the precision in the determination of the degradation curve could be improved by taking more samples. Furthermore to having more samples we can know the exact moment in which the process has reached the total decolorization, or the desired percentage. Moreover, it allows in the determination of the degradation to control the dynamics of the process.

In this chapter we developed a simple non-invasive online monitoring technique for photocatalytic reactors based on the detection of the variations in the decolorization of textile dyes by exploiting the light scattering produced by the photocatalyst in suspension.

The presented online monitoring technique, operates regardless of the geometry or dimensions of the reactor. For the conducted experimental scenarios, lighting source remained external; nevertheless, this technique also can be applied in photoreactors with traditional immersive lighting.

By exploiting the light scattering physical process, it can be achieved the online monitoring of laboratory scale photoreactors (mini and micro reactors), while avoiding the use of supplementary procedures during the photocatalytic process, as is the case of reactors with optical modified characteristics (that permit lighting filtering techniques), or the use of immobilized photocatalysts.

Although for the experimental scenarios presented in this chapter a white light lamp was used, it is also possible to use other types of lighting sources (e.g., laser or LED). Thus, since

it is also possible the degradation assessment in the ultraviolet zone, the online monitoring is not only restricted to decolorization processes, allowing the online degradation monitoring for different applications (e.g., organic matter monitoring).

For this line of research, future work can be focused on developing and implementing automatic control systems that enable the deactivation of the lightning source when the sample reaches the desired degradation percentage, avoiding unnecessary energy consumption; as well as using in-situ monitoring to analyze different types of contaminants.

Chapter 7. CONCLUSIONS AND FUTURE WORK

7.1 General conclusions

- A methodology has been generated for the replacement of conventional lamps by LED Arrays with low energy consumption.

- Using optimized lighting, energy consumption has been reduced, as well as the time for decolorization of textile waters.

- In-situ monitoring in reactors with photocatalyst in suspension dispenses with the implementation of filtering or centrifugation processes, as well as the alteration of current reactors to eliminate the catalyst during the photocatalytic process. In addition, waste of photocatalyst is avoided by removing it before finishing the degradation process.

7.2 Future work

- The results obtained during this research project have been obtained after the common work between the research groups Nonlinear Dynamics, Nonlinear Optics and Lasers (DONLL), Motion Control and Industrial Applications (MCIA) and the collaboration with the Institute of Textile Research and Industrial Cooperation of Terrassa (INTEXTER), who have analyzed the data obtained and provided the chemical agents that have been used. Therefore, the results and future work are of great interest for the three groups.

- The methodology with uniform irradiance models could be improved using genetic algorithms that provide specific arrangements for each reactor surface. The MCIA group has Professors who have worked with different optimization algorithms, including genetic algorithms, therefore, the generation of a new lighting array with a unique shape can be applied soon.

- The signal obtained in non-invasive monitoring can be used to control many parameters of the process, for example, if working with water that does not require total degradation, it could be established to reach a certain threshold to stop the process, or if it is used in chain reactors it could be automated to move on to the next process. The MCIA group is currently working with signal processing for process control, therefore, continuing to work with this type of sensors is under analysis.

Chapter 8. THESIS RESULTS DISSEMINATION

8.1 Journals

Tecilli Tapia, Valentina Buscio, Jose Trull and Vicent Sala, "Performance Analysis and Methodology for replacing conventional lamps by optimized LED arrays for Photocatalytic Processes" in *Chemical Engineering Research and Design*.

Under review since February 2019

Impact factor: 2.795

Tecilli Tapia, Jose Trull, and Luis Romeral, "In-situ decolorization monitoring of textile dyes for an optimized UV-LED/TiO_2 reactor " in *Catalysts*.

Under review (minor revisions)

Impact factor: 3.444

8.2 Congresses

Tapia-Tlatelpa, T.; Trull, J.; Sala, V.; Romeral, L., "Methodology for lighting optimization applied to photocatalytic reactors", in Proceedings of the Numerical Simulation of Optoelectronic Devices (NUSOD); 2019; pp. 31–32.

ISBN: 9781728116471

REFERENCES

1. Organization World Health Nota descriptiva N. 391. *World Heal. Organ.* 2015.

2. Sogaard, E.G. *Chemistry of advanced Environmental Prurification Processes of Water: Fundamentals and Applications*; Sogaard, E.G., Ed.; First.; Elsevier B. V.: Amsterdam, 2014; ISBN 9788578110796.

3. Diario Oficial De Las Comunidades Europeas Directiva 2000/60/CE del Parlamento Europeo y del Consejo. *D. Of. Las Comunidades Eur.* 2000, 1–73.

4. Bilińska, L.; Gmurek, M.; Ledakowicz, S. Comparison between industrial and simulated textile wastewater treatment by AOPs – Biodegradability, toxicity and cost assessment. *Chem. Eng. J.* **2016**, *306*, 550–559.

5. Holkar, C.R.; Jadhav, A.J.; Pinjari, D. V.; Mahamuni, N.M.; Pandit, A.B. A critical review on textile wastewater treatments: Possible approaches. *J. Environ. Manage.* **2016**, *182*, 351–366.

6. Ozturk, E.; Koseoglu, H.; Karaboyaci, M.; Yigit, N.O.; Yetis, U.; Kitis, M. Sustainable textile production: cleaner production assessment/eco-efficiency analysis study in a textile mill. *J. Clean. Prod.* **2016**, *138*, 248–263.

7. Maučec, D.; Šuligoj, A.; Ristić, A.; Dražić, G.; Pintar, A.; Tušar, N.N. Titania versus zinc oxide nanoparticles on mesoporous silica supports as photocatalysts for removal of dyes from wastewater at neutral pH. *Catal. Today* **2017**, *310*, 32–41.

8. Rahman, A.; Urabe, T.; Kishimoto, N. Color Removal of Reactive Procion Dyes by Clay Adsorbents. *Procedia Environ. Sci.* **2013**, *17*, 270–278.

9. Meerbergen, K.; Crauwels, S.; Willems, K.A.; Dewil, R.; Van Impe, J.; Appels, L.; Lievens, B. Decolorization of reactive azo dyes using a sequential chemical and activated sludge treatment. *J. Biosci. Bioeng.* **2017**, *124*, 668–673.

10. Jo, W.K.; Tayade, R.J. Recent developments in photocatalytic dye degradation upon irradiation with energy efficient light emitting diodes. *Chinese J. Catal.* **2014**, *35*, 1781–1792.

11. Buscio, V.; Brosillon, S.; Mendret, J.; Crespi, M.; Gutiérrez-Bouzán, C. Photocatalytic Membrane Reactor for the Removal of C.I. Disperse Red 73. *Materials (Basel).* **2015**, *8*, 3633–3647.

12. Mendoza-Basilio, C.A.; Yee-Madeira, H.; Ramirez-Rodriguez, T.; Colindres, P. Oxidation of textile dye reactive yellow 84 in aqueous solution in order to reuse treated water. *Rev. Mex. Ing. Química* **2017**, *16*, 581–589.

13. Gümüş, D.; Akbal, F. Photocatalytic Degradation of Textile Dye and Wastewater. *Water, Air, Soil Pollut.* **2011**, *216*, 117–124.

14. Ertugay, N.; Acar, F.N. Removal of COD and color from Direct Blue 71 azo dye wastewater by Fenton's oxidation: Kinetic study. *Arab. J. Chem.* **2017**, *10*, S1158–S1163.

15. UNECE Fashion and the SDGs: what role for the UN?; Geneva, 2018.

16. (CAR/PL) *Prevención de la contaminación Industria textil en los países del Mediterráneo*; España, 2002;

17. Jin, X.C.; Liu, G.Q.; Xu, Z.H.; Tao, W.Y. Decolorization of a dye industry effluent by Aspergillus fumigatus XC6. *Appl. Microbiol. Biotechnol.* **2007**, *74*, 239–243.

18. Robinson, T.; Mcmullan, G.; Marchant, R.; Nigam, P. Remediation of dyes in textile effluent : a critical review on current treatment technologies with a proposed alternative. **2001**, *77*, 247–255.

19. Andreozzi, R. Advanced oxidation processes (AOP) for water purification and recovery. *Catal. Today* **1999**, *53*, 51–59.

20. Bethi, B.; Sonawane, S.H.; Rohit, G.S.; Holkar, C.R.; Pinjari, D. V.; Bhanvase, B.A.; Pandit, A.B.

Investigation of TiO_2 photocatalyst performance for decolorization in the presence of hydrodynamic cavitation as hybrid AOP. *Ultrason. Sonochem.* **2016**, *28*, 150–160.

21. Bilińska, L.; Gmurek, M.; Ledakowicz, S. Textile wastewater treatment by AOPs for brine reuse. *Process Saf. Environ. Prot.* **2017**, *109*, 420–428.

22. Herrmann, J.M. Fundamentals and misconceptions in photocatalysis. *J. Photochem. Photobiol. A Chem.* **2010**, *216*, 85–93.

23. Herrmann, J.-M. Heterogeneous photocatalysis: fundamentals and applications to the removal of various types of aqueous pollutants. *Catal. Today* **1999**, *53*, 115–129.

24. Trapido, M. Ozone-based advanced oxidation processes. *Encycl. Life Support Syst.* **2008**, 1–17.

25. Gaya, U.I.; Abdullah, A.H. Heterogeneous photocatalytic degradation of organic contaminants over titanium dioxide: A review of fundamentals, progress and problems. *J. Photochem. Photobiol. C Photochem. Rev.* **2008**, *9*, 1–12.

26. Gogate, P.R.; Pandit, A.B. A review of imperative technologies for wastewater treatment I: Oxidation technologies at ambient conditions. *Adv. Environ. Res.* **2004**, *8*, 501–551.

27. Malato, S.; Fernandez Ibanez, P.; Maldonado, M.I.; Blanco, J.; Gernjak, W. Decontamination and disinfection of water by solar photocatalysis: Recent overview and trends. *Catal. Today* **2009**, *147*, 1–59.

28. Herrmann, J.M. Heterogeneous photocatalysis: State of the art and present applications. *Top. Catal.* **2005**, *34*, 49–65.

29. Ferreira, L.C.; Lucas, M.S.; Fernandes, J.R.; Tavares, P.B. Photocatalytic oxidation of Reactive Black 5 with UV-A LEDs. *J. Environ. Chem. Eng.* **2016**, *4*, 109–114.

30. Gągol, M.; Przyjazny, A.; Boczkaj, G. Wastewater treatment by means of advanced oxidation processes based on cavitation – A review. *Chem. Eng. J.* **2018**, *338*, 599–627.

31. Damodar, R.A.; You, S.J. Performance of an integrated membrane photocatalytic reactor for the removal of Reactive Black 5. *Sep. Purif. Technol.* **2010**, *71*, 44–49.

32. Chong, M.N.; Jin, B.; Chow, C.W.K.; Saint, C. Recent developments in photocatalytic water treatment technology: a review. *Water Res.* **2010**, *44*, 2997–3027.

33. Yoshizawa, T. *Handbook of Optical metrology: Principles and Applications*; Yoshizawa, T., Ed.; Second.; CRC Press: Japan, 2015; ISBN 9781466573611.

34. Cassano, A.E.; Martin, C.A.; J., B.R.; Alfano, O.M. Photoreactor Analysis and Design : Fundamentals and Applications. *Ind. Eng. Chem. Res.* **1995**, *34*, 2155–2201.

35. Hernandez Ramirez, A.; Medina Ramirez, I. Semiconducting Materials. In *Photocatalytic semiconductors: Synthesis, Characterization, and Environmental Applications*; Hernández Ramírez, A., Medina Ramírez, I., Eds.; Springer International Publishing Switzerland: Switzerland, 2015; p. 289 ISBN 9783319109985.

36. Kormann, C.; Bahnemann, D.W.; Hoffmann, M.R. Environmental Photochemistry - Is Iron-Oxide (Hematite) an Active Photocatalyst - a Comparative-Study - Alpha-Fe2O3, ZnO, TiO2. *J. Photochem. Photobiol. a-Chemistry* **1989**, *48*, 161–169.

37. Etacheri, V.; Di Valentin, C.; Schneider, J.; Bahnemann, D.; Pillai, S.C. Visible-light activation of TiO_2 photocatalysts: Advances in theory and experiments. *J. Photochem. Photobiol. C Photochem. Rev.* **2015**, *25*, 1–29.

38. Hashimoto, K.; Irie, H.; Fujishima, A. TiO2 Photocatalysis: A Historical Overview and Future Prospects. *AAPPS Bull.* **2007**, *17*, 12–28.

39. Ohno, T.; Sarukawa, K.; Tokieda, K.; Matsumura, M. Morphology of a TiO_2 Photocatalyst (Degussa, P-25) Consisting of Anatase and Rutile Crystalline Phases. *J. Catal.* **2001**, *203*, 82–86.

40. Shan, A.Y.; Ghazi, T.I.M.; Rashid, S.A. Immobilisation of titanium dioxide onto supporting materials in heterogeneous photocatalysis: A review. *Appl. Catal. A Gen.* **2010**, *389*, 1–8.

41. Manassero, A.; Satuf, M.L.; Alfano, O.M. Evaluation of UV and visible light activity of TiO_2 catalysts for water remediation. *Chem. Eng. J.* **2013**, *225*, 378–386.

42. Bilal, M.; Rasheed, T.; Iqbal, H.M.N.; Li, C.; Wang, H.; Hu, H.; Wang, W.; Zhang, X. Photocatalytic degradation, toxicological assessment and degradation pathway of C.I. Reactive Blue 19 dye. *Chem. Eng. Res. Des.* **2018**, *129*, 384–390.

43. Visa, T.; Sanchez, M.; Lopez-Grimau, V.; Navarro, R.; Reche, S.; Carmen Gutierrez-Bouzan, M. Photocatalysis with titanium dioxide to remove colour of exhausted reactive dyebaths without pH modification. *Desalin. Water Treat.* **2012**, *45*, 91–99.

44. Braslavsky, S.E. Glossary of terms used in photochemistry. *Pure Appl. Chem.* **2007**, *79*, 293–465.

45. Tokode, O.; Prabhu, R.; Lawton, L.A.; Robertson, P.K.J. UV LED Sources for Heterogeneous Photocatalysis. In *Environmental Photochemistry Part III*; Bahnemann, D.W., Robertson, P.K.J., Eds.; Springer- Verlag Berlin Heidelberd: Berlin, 2015; pp. 159–180 ISBN 3-540-00269-3.

46. McDermott, S.L.; Walsh, J.E.; Howard, R.G. A comparison of the emission characteristics of UV-LEDs and fluorescent lamps for polymerisation applications. *Opt. Laser Technol.* **2008**, *40*, 487–493.

47. Bouchy, M.; Zahraa, O. Photocatalytic reactors. *Int. J. Photoenergy* **2003**, *5*, 191–197.

48. Chen, H.W.; Ku, Y.; Wu, C.Y. Effect of LED optical characteristics on temporal behavior or o-cresol decomposition by UV TiO2 process. *J. Chem. Technol. Biotechnol.* **2007**, *82*, 626–635.

49. Natarajan, T.S.; Natarajan, K.; Bajaj, H.C.; Tayade, R.J. Energy efficient UV-LED source and TiO_2 nanotube array-based reactor for photocatalytic application. *Ind. Eng. Chem. Res.* **2011**, *50*, 7753–7762.

50. Repo, E.; Rengaraj, S.; Pulkka, S.; Castangnoli, E.; Suihkonen, S.; Sopanen, M.; Sillanpaa, M. Photocatalytic degradation of dyes by CdS microspheres under near UV and blue LED radiation. *Sep. Purif. Technol.* **2013**, *120*, 206–214.

51. Natarajan, K.; Natarajan, T.S.; Bajaj, H.C.; Tayade, R.J. Photocatalytic reactor based on UV-LED/TiO_2 coated quartz tube for degradation of dyes. *Chem. Eng. J.* **2011**, *178*, 40–49.

52. Leblebici, M.E.; Stefanidis, G.D.; Van Gerven, T. Comparison of photocatalytic space-time yields of 12 reactor designs for wastewater treatment. *Chem. Eng. Process. Process Intensif.* **2015**, *97*, 106–111.

53. Ohtani, B.; Prieto-Mahaney, O.O.; Li, D.; Abe, R. What is Degussa (Evonic) P25? Crystalline composition analysis, reconstruction from isolated pure particles and photocatalytic activity test. *J. Photochem. Photobiol. A Chem.* **2010**, *216*, 179–182.

54. Fox, M.A.; Dulay, M.T. Heterogeneous Photocatalysis. *Chem. Rev.* **1993**, *93*, 341–357.

55. Jamali, A.; Vanraes, R.; Hanselaer, P.; Van Gerven, T. A batch LED reactor for the photocatalytic degradation of phenol. *Chem. Eng. Process. Process Intensif.* **2013**, *71*, 43–50.

56. Kim, S.H.; Lee, S.W.; Lee, G.M.; Lee, B.T.; Yun, S.T.; Kim, S.O. Monitoring of TiO_2-catalytic UV-LED photo-oxidation of cyanide contained in mine wastewater and leachate. *Chemosphere* **2016**, *143*, 106–114.

57. Chen, H.W.; Ku, Y.; Irawan, A. Photodecomposition of o-cresol by UV-LED/TiO_2 process with controlled periodic illumination. *Chemosphere* **2007**, *69*, 184–190.

58. McCullagh, C.; Skillen, N.; Adams, M.; Robertson, P.K.J. Photocatalytic reactors for environmental remediation: A review. *J. Chem. Technol. Biotechnol.* **2011**, *86*, 1002–1017.

59. Shie, J.L.; Lee, C.H.; Chiou, C.S.; Chang, C.T.; Chang, C.C.; Chang, C.Y. Photodegradation kinetics of formaldehyde using light sources of UVA, UVC and UVLED in the presence of composed silver titanium oxide photocatalyst. *J. Hazard. Mater.* **2008**, *155*, 164–172.

60. Chen, H.C.; Wu, G.Y. Investigation of irradiance efficiency for LED phototherapy with different arrays. *Opt. Commun.* **2010**, *283*, 4882–4886.

61. Wang, X. LED ring array light source design and uniform illumination properties analysis. *Opt. - Int. J. Light Electron Opt.* **2017**, *140*, 273–281.

62. Su, Z.; Xue, D.; Ji, Z. Designing LED array for uniform illumination distribution by simulated annealing algorithm. *Opt. Express* **2012**, *20*, A843.

63. Ramane, D.; Shaligram, A. Optimization of multi-element LED source for uniform illumination of plane surface. *Opt. Express* **2011**, *19 Suppl 4*, A639–A648.

64. Moreno, I.; Tzonchev, R.I. Designing light-emitting diode arrays for uniform near-field irradiance. *Appl. Opt.* **2006**, *45*, 2265–2272.

65. Ahmad, A.L.; Puasa, S.W. Reactive dyes decolourization from an aqueous solution by combined coagulation/micellar-enhanced ultrafiltration process. *Chem. Eng. J.* **2007**, *132*, 257–265.

66. Lanzarini-Lopes, M.; Garcia-Segura, S.; Hristovski, K.; Westerhoff, P. Electrical energy per order and current efficiency for electrochemical oxidation of p-chlorobenzoic acid with boron-doped diamond anode. *Chemosphere* **2017**, *188*, 304–311.

67. Miklos, D.B.; Remy, C.; Jekel, M.; Linden, K.G.; Drewes, J.E.; Hübner, U. Evaluation of advanced oxidation processes for water and wastewater treatment – A critical review. *Water Res.* **2018**, *139*, 118–131.

68. Bolton, J.R.; Bircher, K.G.; Tumas, W.; Tolman, C.A. Figures-of-merit for the technical development and application of advanced oxidation technologies for both electric- and solar-driven systems (IUPAC Technical Report). *Pure Appl. Chem.* **2001**, *73*, 627–637.

69. Muruganandham, M.; Selvam, K.; Swaminathan, M. A comparative study of quantum yield and electrical energy per order (E_{EO}) for advanced oxidative decolourisation of reactive azo dyes by UV light. *J. Hazard. Mater.* **2007**, *144*, 316–322.

70. Daneshvar, N.; Aber, S.; Seyed Dorraji, M.S.; Khataee, A.R.; Rasoulifard, M.H. Photocatalytic degradation of the insecticide diazinon in the presence of prepared nanocrystalline ZnO powders under irradiation of UV-C light. *Sep. Purif. Technol.* **2007**, *58*, 91–98.

71. Dominguez, S.; Rivero, M.J.; Gomez, P.; Ibañez, R.; Ortiz, I. Kinetic modeling and energy evaluation of sodium dodecylbenzenesulfonate photocatalytic degradation in a new LED reactor. *J. Ind. Eng. Chem.* **2016**, *37*, 237–242.

72. Rasoulifard, M.H.; Marandi, R.; Majidzadeh, H.; Bagheri, I. Ultraviolet Light-Emitting Diodes and Peroxydisulfate for Degradation of Basic Red 46 from Contaminated Water. *Environ. Eng. Sci.* **2011**, *28*, 229–235.

73. Khezrianjoo, S.; Revanasiddappa, H.D. Effect of operational parameters and kinetic study on the photocatalytic degradation of m-cresol purple using irradiated ZnO in aqueous medium. *Water Qual. Res. J. Canada* **2016**, *51*, 69–78.

74. Dalapati, P.; Manik, N.B.; Basu, A.N. Effect of temperature on the intensity and carrier lifetime of an AlGaAs based red light emitting diode. *Opt. Quantum Electron.* **2015**, *47*, 1227–1238.

75. Cao, X.A.; LeBoeuf, S.F. Current and temperature dependent characteristics of deep-ultraviolet light-emitting diodes. *IEEE Trans. Electron Devices* **2007**, *54*, 3414–3417.

76. Reynolds, K.J.; De Kock, J.P.; Tarassenko, L.; Moyle, J.T.B. Temperature dependence of led and its theoretical effect on pulse oximetry. *Br. J. Anaesth.* **1991**, *67*, 638–643.

77. Murtaza, G.; Senior, J.M. Dual Wavelength Referenced LED Based Sensors. *IEEE Photonics Technol. Lett.* **1994**, *6*, 1020–1022.

78. Chiu, Y.-H.; Chang, T.-F.M.; Chen, C.-Y.; Sone, M.; Hsu, Y.-J. Mechanistic Insights into Photodegradation of Organic Dyes Using Heterostructure Photocatalysts. *Catalysts* **2019**, *9*, 1–32.

79. Ibhadon, A.; Fitzpatrick, P. Heterogeneous Photocatalysis: Recent Advances and Applications. *Catalysts* **2013**, *3*, 189–218.

80. van Walsem, J.; Roegiers, J.; Modde, B.; Lenaerts, S.; Denys, S. Determination of intrinsic kinetic parameters in photocatalytic multi-tube reactors by combining the NTUm-method with radiation field modelling. *Chem. Eng. J.* **2018**, *354*, 1042–1049.

81. Dougna, A.A.; Gombert, B.; Kodom, T.; Djaneye-Boundjou, G.; Boukari, S.O.B.; Leitner, N.K.V.;

Bawa, L.M. Photocatalytic removal of phenol using titanium dioxide deposited on different substrates: Effect of inorganic oxidants. *J. Photochem. Photobiol. A Chem.* **2015**, *305*, 67–77.

82. Bukman, L.; de Freitas, C.F.; Caetano, W.; Fernandes, N.R.C.; Hioka, N.; Batistela, V.R. Kinetic spectrophotometric method for real-time monitoring of ultraviolet photoreactions: A mini-photoreactor. *Spectrochim. Acta - Part A Mol. Biomol. Spectrosc.* **2019**, *211*, 330–335.

83. Ren, Y.; Jing, D. Study on particle and photonic flux distributions in a magnetically stirred photocatalytic reactor. *J. Photonics Energy* **2015**, *5*, 052097.

84. Ung-Medina, F.; Villicaña-Méndez, M.; Huirache-Acuña, R.; Cortés, J.A. Experimental methodology to calculate the local relative light intensity in heterogeneous TiO_2/UV-A photocatalytic reactors. *Chem. Eng. Res. Des.* **2015**, *97*, 28–35.

85. Davididou, K.; McRitchie, C.; Antonopoulou, M.; Konstantinou, I.; Chatzisymeon, E. Photocatalytic degradation of saccharin under UV-LED and blacklight irradiation. *J. Chem. Technol. Biotechnol.* **2017**, *93*, 269–276.

86. Casado, C.; Marugán, J.; Timmers, R.; Muñoz, M.; van Grieken, R. Comprehensive multiphysics modeling of photocatalytic processes by computational fluid dynamics based on intrinsic kinetic parameters determined in a differential photoreactor. *Chem. Eng. J.* **2017**, *310*, 368–380.

87. Martín-Sómer, M.; Pablos, C.; van Grieken, R.; Marugán, J. Influence of light distribution on the performance of photocatalytic reactors: LED vs mercury lamps. *Appl. Catal. B Environ.* **2017**, *215*, 1–7.

88. Jo, W.K.; Eun, S.S.; Shin, S.H. Feasibility of light-emitting diode uses for annular reactor inner-coated with TiO_2 or nitrogen-doped TiO_2 for control of dimethyl sulfide. *Photochem. Photobiol.* **2011**, *87*, 1016–1023.

89. Long, T.; Xu, Y.; Lv, X.; Ran, J.; Yang, S.; Xu, L. Fabrication of the annular photocatalytic reactor using large-sized freestanding titania-silica monolithic aerogel as the catalyst for degradation of glyphosate. *Mater. Des.* **2018**, *159*, 195–200.

90. Ranjbar, P.Z.; Ayati, B.; Ganjidoust, H. Kinetic study on photocatalytic degradation of Acid Orange 52 in a baffled reactor using TiO_2 nanoparticles. *J. Environ. Sci. (China)* **2019**, *79*, 213–224.

91. Boyjoo, Y.; Ang, M.; Pareek, V. CFD simulation of a pilot scale slurry photocatalytic reactor and design of multiple-lamp reactors. *Chem. Eng. Sci.* **2014**, *111*, 266–277.

92. Athanasiou, D.A.; Romanos, G.E.; Falaras, P. Design and optimization of a photocatalytic reactor for water purification combining optical fiber and membrane technologies. *Chem. Eng. J.* **2015**.

93. Khodadadian, F.; de la Garza, F.G.; van Ommen, J.R.; Stankiewicz, A.I.; Lakerveld, R. The application of automated feedback and feedforward control to a LED-based photocatalytic reactor. *Chem. Eng. J.* **2019**, *362*, 375–382.

94. Tokode, O.; Prabhu, R.; Lawton, L.A.; Robertson, P.K.J. Controlled periodic illumination in semiconductor photocatalysis. *J. Photochem. Photobiol. A Chem.* **2016**, *319–320*, 96–106.

95. Li, Y.; Lin, B.; Ge, L.; Guo, H.; Chen, X.; Lu, M. Real-time spectroscopic monitoring of photocatalytic activity promoted by graphene in a microfluidic reactor. *Sci. Rep.* **2016**, *6*, 1–9.

96. Tapia-Tlatelpa, T.; Trull, J.; Sala, V.; Romeral, L. Methodology for lighting optimization applied to photocatalytic reactors. In Proceedings of the Numerical Simulation of Optoelectronic Devices (NUSOD); 2019; pp. 31–32.

97. Schneider, O.; Liang, R.; Bragg, L.; Jaciw-Zurakowsky, I.; Fattahi, A.; Rathod, S.; Peng, P.; Servos, M.; Zhou, Y. Photocatalytic Degradation of Microcystins by TiO_2 Using UV-LED Controlled Periodic Illumination. *Catalysts* **2019**, *9*, 181.

98. Nickels, P.; Zhou, H.; Basahel, S.N.; Obaid, A.Y.; Ali, T.T.; Al-Ghamdi, A.A.; El-Mossalamy, E.S.H.; Alyoubi, A.O.; Lynch, S.A. Laboratory scale water circuit including a photocatalytic reactor and a portable in-stream sensor to monitor pollutant degradation. *Ind. Eng. Chem. Res.* **2012**, *51*, 3301–3308.

99. Jo, W.K.; Park, G.T.; Tayade, R.J. Synergetic effect of adsorption on degradation of malachite green dye under blue LED irradiation using spiral-shaped photocatalytic reactor. *J. Chem. Technol. Biotechnol.*

2015, *90*, 2280–2289.

100. Natarajan, T.S.; Thomas, M.; Natarajan, K.; Bajaj, H.C.; Tayade, R.J. Study on UV-LED/TiO_2 process for degradation of Rhodamine B dye. *Chem. Eng. J.* **2011**, *169*, 126–134.

101. McCullagh, C.; Robertson, P.K.J.; Adams, M.; Pollard, P.M.; Mohammed, A. Development of a slurry continuous flow reactor for photocatalytic treatment of industrial waste water. *J. Photochem. Photobiol. A Chem.* **2010**, *211*, 42–46.

102. Reddy, P.A.K.; Reddy, P.V.L.; Kwon, E.; Kim, K.-H.; Akter, T.; Kalagara, S. Recent advances in photocatalytic treatment of pollutants in aqueous media. *Environ. Int.* **2016**, *91*, 94–103.

103. Jo, W.K.; Tayade, R.J. New generation energy-efficient light source for photocatalysis: LEDs for environmental applications. *Ind. Eng. Chem. Res.* **2014**, *53*, 2073–2084.

104. Mortazavian, S.; Saber, A.; James, D.E. Optimization of Photocatalytic Degradation of Acid Blue 113 and Acid Red 88 Textile Dyes in a UV-C/TiO_2 Suspension System: Application of Response Surface Methodology (RSM). *Catalysts* **2019**, *9*, 1–19.

105. Claes, T.; Dilissen, A.; Leblebici, M.E.; Van Gerven, T. Translucent packed bed structures for high throughput photocatalytic reactors. *Chem. Eng. J.* **2019**, *361*, 725–735.

106. Manassero, A.; Satuf, M.L.; Alfano, O.M. Photocatalytic reactors with suspended and immobilized TiO_2: Comparative efficiency evaluation. *Chem. Eng. J.* **2017**, *326*, 29–36.

107. Xiong, P.; Hu, J. Inactivation/reactivation of antibiotic-resistant bacteria by a novel UVA/LED/TiO_2 system. *Water Res.* **2013**, *47*, 4547–4555.

108. Tuncì, S.; Duman, O.; Gürkan, T. Monitoring the decolorization of acid orange 8 and acid red 44 from aqueous solution using Fenton's reagents by online spectrophotometric method: Effect of operation parameters and kinetic study. *Ind. Eng. Chem. Res.* **2013**, *52*, 1414–1425.

109. Sala, M.; López-Grimau, V.; Gutiérrez-Bouzán, C. Photo-electrochemical treatment of reactive dyes in wastewater and reuse of the effluent: Method optimization. *Materials (Basel).* **2014**, *7*, 7349–7365.

110. Namour, P.; Jaffrezic-Renault, N.; Namour, P. Sensors for measuring biodegradable and total organic matter in water. *TrAC - Trends Anal. Chem.* **2010**, *29*, 848–857.

111. Zheng, X.; Shen, Z.-P.; Shi, L.; Cheng, R.; Yuan, D.-H. Photocatalytic Membrane Reactors (PMRs) in Water Treatment: Configurations and Influencing Factors. *Catalysts* **2017**, *7*, 224.

112. Cao, F.; Li, H.; Chao, H.; Zhao, L.; Guo, L. Optimization of the concentration field in a suspended photocatalytic reactor. *Energy* **2014**, *74*, 140–146.

113. Romero, R.L.; Alfano, O.M.; Cassano, A.E. Cylindrical Photocatalytic Reactors. Radiation Absorption and Scattering Effects Produced by Suspended Fine Particles in an Annular Space. *Ind. Eng. Chem. Res.* **1997**, 3094–3109.

114. Cabrera, M.I.; Alfano, O.M.; Cassano, A.E. Absorption and Scattering Coefficients of Titanium Dioxide Particulate Suspensions in Water. *J. Phys. Chem.* **1996**, *100*, 20043–20050.

115. Li Puma, G.; Brucato, A. Dimensionless analysis of slurry photocatalytic reactors using two-flux and six-flux radiation absorption-scattering models. *Catal. Today* **2007**, *122*, 78–90.